JGR Oceans

RESEARCH ARTICLE
10.1029/2020JC016271

Quasi-Biweekly Mode of the Asian Summer Monsoon Revealed in Bay of Bengal Surface Observations

J. Sree Lekha[1], Andrew J. Lucas[2], Jai Sukhatme[1], Jossia K. Joseph[3], M. Ravichandran[4], N. Suresh Kumar[5], J. Thomas Farrar[6], and D. Sengupta[7]

[1]Centre for Atmospheric and Oceanic Sciences, Indian Institute of Science, Bangalore, India, [2]Scripps Institution of Oceanography and Department of Mechanical and Aerospace Engineering, University of California, San Diego, La Jolla, CA, USA, [3]National Institute for Ocean Technology, Ministry of Earth Sciences, Chennai, India, [4]National Centre for Polar and Ocean Research, Ministry of Earth Sciences, Vasco da Gama, India, [5]Indian National Centre for Ocean Information Services, Ministry of Earth Sciences, Hyderabad, India, [6]Woods Hole Oceanographic Institution, Woods Hole, MA, USA, [7]Centre for Atmospheric and Oceanic Sciences and Divecha Centre for Climate Change, Indian Institute of Science, Bangalore, India

Abstract Asian summer monsoon has a planetary-scale, westward propagating "quasi-biweekly" mode of variability with a 10–25 day period. Six years of moored observations at 18°N, 89.5°E in the north Bay of Bengal (BoB) reveal distinct quasi-biweekly variability in sea surface salinity (SSS) during summer and autumn, with peak-to-peak amplitude of 3–8 psu. This large-amplitude SSS variability is not due to variations of surface freshwater flux or river runoff. We show from the moored data, satellite SSS, and reanalyses that surface winds associated with the quasi-biweekly monsoon mode and embedded weather-scale systems, drive SSS and coastal sea level variability in 2015 summer monsoon. When winds are calm, geostrophic currents associated with mesoscale ocean eddies transport Ganga-Brahmaputra-Meghna river water southward to the mooring, salinity falls, and the ocean mixed layer shallows to 1–10 m. During active (cloudy, windy) spells of quasi-biweekly monsoon mode, directly wind-forced surface currents carry river water away to the east and north, leading to increased salinity at the moorings, and rise of sea level by 0.1–0.5 m along the eastern and northern boundary of the bay. During July–August 2015, a shallow pool of low-salinity river water lies in the northeastern bay. The amplitude of a 20-day oscillation of sea surface temperature (SST) is two times larger within the fresh pool than in the saltier ocean to the west, although surface heat flux is nearly identical in the two regions. This is direct evidence that spatial-temporal variations of BoB salinity influences sub-seasonal SST variations, and possibly SST-mediated monsoon air-sea interaction.

Plain Language Summary The north Bay of Bengal (BoB) is characterized by 1–10 m deep layer of river water, very stable density stratification, and deep isothermal layer warmed by penetration of sunlight below the thin mixed layer. Thermodynamic structure of the upper ocean influences intraseasonal active-break cycles of the summer monsoon and promotes intensification of postmonsoon tropical cyclones by inhibiting storm-induced cooling of sea surface temperature. Hence, it is important to understand the space-time variability of surface salinity in this basin. The quasi-biweekly (10–25 day) oscillation is a prominent mode of the Asian summer monsoon, seen in winds, cloudiness, rainfall and surface heat flux. Six years of mooring observations at 18°N in the north BoB show large amplitude (2–8 psu) changes in surface salinity on quasi-biweekly timescales in summer and autumn. Using moored observations, satellite data and reanalyses, we show that changes in surface winds associated with quasi-biweekly monsoon mode and its embedded low-pressure systems drive large changes in surface salinity and coastal sea level. We show that the response of SST to subseasonal variations of surface heat flux is enhanced in the presence of a thin layer of river water. These observations have important implications for regional air-sea interaction on subseasonal timescales.

Key Points:

- Moored observations show large amplitude quasi-biweekly variability of surface salinity in the north Bay of Bengal
- Mesoscale eddies and shallow wind-driven monsoon currents lead to lateral dispersal of river water
- Shallow, fresh layer enhances sea surface temperature response to surface heat flux on subseasonal timescales

Supporting Information:

- Figure S1
- Figure S2
- Figure S3
- Figure S4
- Figure S5

Correspondence to:
J. Sree Lekha,
sree@iisc.ac.in

Citation:
Sree Lekha, J., Lucas, A. J., Sukhatme, J., Joseph, J. K., Ravichandran, M., Suresh Kumar, N., et al. (2020). Quasi-biweekly mode of the Asian summer monsoon revealed in Bay of Bengal surface observations. *Journal of Geophysical Research: Oceans*, *125*, e2020JC016271. https://doi.org/10.1029/2020JC016271

Received 25 MAR 2020
Accepted 11 NOV 2020

1. Introduction

Surface salinity in the Bay of Bengal (BoB) has a well-defined seasonal cycle, with highest open ocean salinity (generally in the range 33–34 psu) in spring (March–May) and lowest values (24–32 psu) during late summer and autumn (September–November) (R. R. Rao & Sivakumar 2003; Sengupta et al., 2016).

In an annual, areal average, it is the freshest marginal sea in the tropical oceans. Five of the world's 50 largest rivers, the Ganga-Brahmaputra-Meghna (GBM), Irrawady, Krishna, Godavari, and Mahanadi, flow into the northern BoB; discharge from these rain-fed rivers has a pronounced summertime peak (Dai & Trenberth, 2002; Fekete et al., 2002; Papa et al., 2010). Oceanic precipitation also has marked seasonality—in four months during the summer monsoon season (June–September), the northern BoB receives 1.5–2 m of rainfall. The annual excess input of freshwater from river runoff and precipitation over evaporation is ~4,000 km^3 across the 2 million km^2 area of the Bay. Summer rain and runoff from the GBM and the Irrawady keeps the surface salinity of the north bay relatively fresh for nearly three seasons (Papa et al., 2012; Sengupta et al., 2006, 2016). The seasonal cycle and interannual variability of BoB salinity has been extensively studied using *in situ* observations, ocean reanalyses and models (Akhil et al., 2014; Babu et al., 2003; Benshila et al., 2014; Chaitanya et al., 2015; Diansky et al., 2006; Murty et al., 1992; Pant et al., 2015; R. R. Rao & Sivakumar, 2003; Shenoi et al., 2002; Shetye et al., 1993, 1996; Wilson & Riser, 2016). The low-salinity surface water of the BoB has a profound influence on regional air-sea interaction, with impacts on synoptic to intraseasonal monsoon variability across the south Asian region.

It has been argued that the low surface salinity and shallow halocline in the BoB increases the gravitational stability of the water column, helping to keep sea surface temperature (SST) warm, in spite of enhanced surface wind stress in the summer monsoon season (Lucas et al., 2016; Sengupta et al., 2016). During the summer monsoon season, the cooling of Arabian Sea SST is distinctly larger than the cooling of BoB SST—the warm ocean supports intense monsoon rainfall, leading to lower surface salinity in a positive feedback cycle (Gadgil, 2003; Shenoi et al., 2002). The summertime freshwater input in the north BoB leads to a "barrier layer" structure in late summer and autumn, with very shallow surface mixed layers (less than 10 m deep) and a deep subsurface warm layer, created mainly by penetration of incident sunlight below the shallow mixed layer (Prend et al., 2019; Sengupta & Ravichandran, 2001; Vinayachandran et al., 2002). While BoB SST cools due to surface heat loss in winter, the deep warm subsurface layer persists, leading to temperature inversions that can reach 4–5°C (Thadathil et al., 2016).

Powerful postmonsoon tropical cyclones in the north BoB lead to vertical mixing of the upper ocean down to 50 m or so. However, little or no SST cooling is seen under the tracks of postmonsoon (October–November) tropical cyclones in the open ocean, mainly for two reasons: (i) the stable, shallow salinity-dominated density stratification reduces the maximum depth of storm-induced vertical mixing, and (ii) the mixing is confined to the nearly isothermal subsurface warm layer. It is likely that the very rapid intensification characteristic of many BoB cyclones (Mohapatra et al., 2015) is related to the temperature–salinity structure of the upper ocean (Balaguru et al., 2012; Chaudhuri et al., 2019; Neetu et al., 2012; Qiu et al., 2019; Sengupta et al., 2008; Vincent et al., 2014).

The intraseasonal variability (ISV; 10–90 day periods) of BoB salinity is drawing increasing attention in the last decade. Parampil et al. (2010) discovered a prominent intraseasonal signal in salinity data from Argo floats with 5-day sampling in the central and north BoB. They showed that the observed ISV of near-surface salinity is not a response to local freshwater forcing, that is, precipitation minus evaporation ($P - E$), but is mainly due to lateral advection. Analysis of time series observations from the RAMA mooring at 15°N, 90°E also indicates that intraseasonal variations of salinity are mainly due to lateral advection (Rao et al., 2011). Li et al. (2017) show from experiments with the Hybrid Coordinate Ocean Model (HYCOM) that the variability of sea surface salinity (SSS) and near-surface stratification in the northern BoB on 20–90 day timescales is mainly due to advection by wind-driven currents and ocean eddies. Recent studies have detected intraseasonal oscillations of SSS in satellite data. For example, Grunseich et al. (2013) find intraseasonal oscillations with 30–90 day periods in Aquarius SSS in the equatorial Indian Ocean, forced by the Madden Julian Oscillation (MJO). Subrahmanyam et al. (2018), Trott et al. (2019), and Roman-Stork et al. (2019) use spectral analysis of the Soil Moisture Active Passive (SMAP) SSS data during 2015–2017 to detect variability on 30–90 day, quasi-biweekly (10–20 day) and shorter scales in the BoB, although they do not explore the mechanisms in any detail.

Observations show that BoB SST has large-amplitude intraseasonal oscillations which move northward in a coherent manner with intraseasonal changes in large-scale atmospheric convection and surface heat flux during the summer monsoon season (Sengupta et al., 2001; Vecchi & Harrison, 2002). The shallow, low

salinity mixed layer in the north BoB favors 30–40 day SST oscillations with peak-to-peak amplitudes often reaching 2–3°C. The SST oscillations are mainly a response to alternating positive and negative net surface heat flux (typically +80 to −80 Wm^{-2}) associated with the active-break cycles of the summer monsoon (Parampil et al., 2016; Sengupta & Ravichandran, 2001; Vialard et al., 2012), with a more modest contribution from lateral advection (Buckley et al., 2020). From spectral analysis of Tropical Rainfall Measuring Mission Microwave Imager (TMI) SST during the summer monsoon season, Parekh et al. (2004) found a dominant 30–60 day mode, and a secondary 8–16 day mode of variability in the BoB. They attributed the 30–60 day SST variability to forcing by the monsoon active-break cycle, and the 8–16 day variability to convection associated with synoptic weather systems. Distinct SST variability on quasi-biweekly timescale was noted nearly 15 years ago, and attributed mainly to surface radiative fluxes and wind forcing (Agarwal et al., 2007; Han et al., 2006).

The alternating episodes of warming and cooling of the north bay results in time-varying spatial gradients of SST between the northern bay and central/southern bay—the large-scale north-south SST gradient is thought to actively influence the slowly northward moving summer monsoon cloud and precipitation bands (Fu et al., 2003; Goswami, 2012; Joseph & Sabin, 2008; Shankar et al., 2007; Vecchi & Harrison, 2002). Many model studies indicate that active coupling with the ocean influences the monsoon intraseasonal oscillation, leading to more realistic structure and propagation of large-scale atmospheric convection and rainfall (e.g., DeMott et al., 2014; Fu et al., 2007; Goswami, 2012). The modeling study of Li et al. (2017) shows that near-surface salinity stratification in the BoB influences the evolution of SST on intraseasonal timescales, and therefore monsoon air-sea interaction. The influence of smaller scale variations of ocean mixed layer depth and SST gradients on air-sea interaction has just begun to be explored. Samanta et al. (2018) used a high-resolution regional atmospheric model coupled to a slab ocean to show that a shallow, low-salinity mixed layer in the northwestern BoB is anomalously warm, in agreement with observations. Sensitivity experiments indicate that spatial gradients of SST on order 100 km scales can enhance seasonal mean precipitation over the Indian subcontinent through a significant increase in intense monsoon rainfall events.

The quasi-biweekly (10–25 day period) variability of the monsoon is an integral component of tropical ISV . The westward moving quasi-biweekly mode is associated with atmospheric moist convection in the 10°–30° latitude band in both hemispheres (Chen & Chen, 1993; Kikuchi & Wang, 2009; Krishnamurti & Bhalme, 1976). During the boreal summer monsoon season, the quasi-biweekly mode has a zonal wavelength of 4,000–6,000 km, and propagates westward at 4–5 m/s across the tropical Pacific and Indian oceans. It has an equatorial Rossby wave-like double vortex structure, except that the line of symmetry between the counter-rotating vortices generally lies at 5–15°N latitude in summer, rather than on the equator (Chatterjee & Goswami, 2004; Chen & Chen, 1993). The quasi-biweekly mode has significant influence on the variability of the south Asian monsoon (Fujinami et al., 2014; Krishnamurti & Bhalme, 1976) as well as summer rainfall, winds and vorticity in the equatorial Pacific ocean, southeast Asia and the South China Sea (Chen & Sui, 2010; Wang & Chen, 2017; Wang et al., 2009; Wang & Zhang, 2019).

In the BoB and contiguous land regions, quasi-biweekly variability has been observed in atmospheric winds, outgoing longwave radiation, surface pressure, and rainfall in the summer monsoon season (Goswami, 2012). Cyclonic vorticity associated with the northern vortex of the quasi-biweekly mode leads to enhanced frequency of genesis of synoptic-scale low pressure systems in the north BoB and adjacent land (Goswami et al., 2003). Fujinami et al. (2014) found distinct quasi-biweekly variability in summer monsoon rainfall in Bangladesh, Myanmar, the BoB and eastern India, which are associated with characteristic changes in low-level wind and vorticity anomalies.

This study focuses on the imprint of the quasi-biweekly monsoon mode on open ocean salinity and coastal sea level in the northern BoB. We use six years of hourly data from open ocean moorings, located near 18°N, 89.5°E, nearly 500 km from the mouths of the GBM and Irrawady rivers. We use spectral analysis of the moored surface salinity and wind observations to identify dominant timescales. We then analyse the moored observations, in combination with satellite data and an ocean analysis dataset, to focus on the distinct quasi-biweekly response of surface salinity to monsoon winds and ocean currents during the 2015 summer monsoon season. We show that eddy stirring and the shallow wind-driven flow provide a simple explanation for the observed changes of surface salinity and sea level in the northern BoB. The outline of

the paper is as follows: In Section 2, we describe the datasets used in this study. In Section 3, we present the observed variability of winds, sea surface salinity and related quantities, based mainly on the six-year long mooring record. A detailed analysis of quasi-biweekly variability of winds, rainfall, and sea surface salinity and sea level during the 2015 summer monsoon is presented in Section 4. In Section 5, we discuss the observed sea surface temperature response to surface heat flux in the presence of a thin, fresh layer, followed by a summary in Section 6.

2. Data

We use hourly observations from four moorings deployed by the Indian National Center for Ocean Information Services (INCOIS; Sengupta et al., 2016), Woods Hole Oceanographic Institution (WHOI, Weller et al., 2016) and the National Institute of Ocean Technology (NIOT; Venkatesan et al., 2013). The INCOIS mooring at 18°N, 89.5°E was deployed from November 6, 2009 to November 22, 2010, and again from January 1, 2013 to December 2014. This mooring had temperature (T), salinity (S) and current measurements at several depths in the upper 100 m; it did not carry meteorological sensors. It was replaced by a WHOI mooring, deployed at 18.01°N, 89.45°E from December 8, 2014 to January 29, 2016. The two NIOT moorings BD08 at 17.88°N, 89.67°E, and BD09 at 18.12°N, 89.67°E, have been operational since June 2013. The distances between the INCOIS (or WHOI) mooring and the two NIOT moorings are 21–27 km (Figure 2a). All the moorings are equipped with the Seabird SBE37 MicroCAT CT sensors to measure temperature and salinity. The accuracy of the CT sensor is 0.002°C for temperature and 0.0003 S/m for conductivity; salinity estimated from temperature and conductivity has an accuracy of 0.02 psu.

In order to study near-surface variability of the ocean and atmosphere, we use hourly temperature and salinity measurements at the shallowest available depth (1, 4 or 5 m) on each of the WHOI, INCOIS and NIOT moorings; hourly surface winds measured at 3 m height on the WHOI and NIOT moorings (Gill Instruments Wind Observer II Ultrasonic Anemometer) extrapolated to 10 m height. The shallowest ocean currents are measured using a Nortek Aquadopp current meter at 3.5 m depth on the WHOI mooring, and a Teledyne RDI DVS current meter at 1.2 m depth on the NIOT moorings.

We use daily discharge at the GBM river mouth estimated from *in situ* water level measured at two stations (Hardinge, Ganga and Bahadurabad, Brahmaputra) and stage-discharge relationships derived from satellite altimeter data (Papa et al., 2010; available 1995–2013). In addition, we use the following gridded datasets: Daily SSS version 3 from the SMAP satellite, based on 8-day running mean SSS on a 0.25° spatial grid (Fore et al., 2016; April 2015–present); daily 0.25° satellite microwave-based sea surface temperature (OI SST) from Remote Sensing Systems (Udaya Bhaskar et al., 2013); daily 0.25° radiative fluxes from TropFlux (Kumar et al., 2012, 1998–present); daily 0.25° rainfall from the multisatellite Tropical Rainfall Measuring Mission (TRMM) 3B42v7 dataset (Huffman et al., 2007, 1998–present) and daily 0.25° AVISO surface geostrophic currents (1992–present).

In addition to moored observations and satellite data, we use selected data from atmospheric and ocean reanalyses: Daily 850 hPa winds and surface wind stress on a 0.5° × 0.625° spatial grid from the Modern-Era Retrospective analysis for Research and Applications Version 2 (MERRA-2) product (Gelaro et al., 2017); and daily sea level, surface salinity (at 0.5 m depth), mixed depth estimates and upper ocean currents from the global ocean physics analysis and forecast product (Global_Analysis_Forecast_PHY_001_030). The ocean analysis uses the Nucleus for European Modeling of the Ocean (NEMO) model v3.1 with 1/12° horizontal resolution and 50 vertical levels; the temporal coverage is 1993–2018. Satellite altimeter data from AVISO, all available *in situ* temperature and salinity profiles including Argo data, and Operational Sea Surface Temperature and Ice Analysis (OSTIA) SST which comprises of *in situ* observations and satellite data provided by the Group for High Resolution Sea Surface Temperature (GHRSST) are assimilated, and atmospheric forcing from the European Center for Medium-Range Weather Forecasts (ECMWF) Integrated Forecast System (IFS) is used to produce daily analysis and 10-day forecasts each day; the daily dataset is a time average of the analysis and model forecast. This product does not assimilate satellite SSS, and the NEMO model configuration does not include tides (Chassignet et al., 2018).

3. Multi-year Observations From Moorings

Surface temperature and salinity from the north BoB moorings have a marked seasonal cycle (Figures 1a–1c; Schott & McCreary, 2009; Rao & Sivakumar, 2003). We note the main features of the seasonal cycle of SST and SSS, as seen in the moored observations. SST warms by 5–6°C in the spring season February–April (Sengupta et al., 2002), and cools by 4–5°C in autumn and winter, that is, mid-October to January in most years (Figure 1b; Thadathil et al., 2016). Surface salinity is lowest in August–October due to the

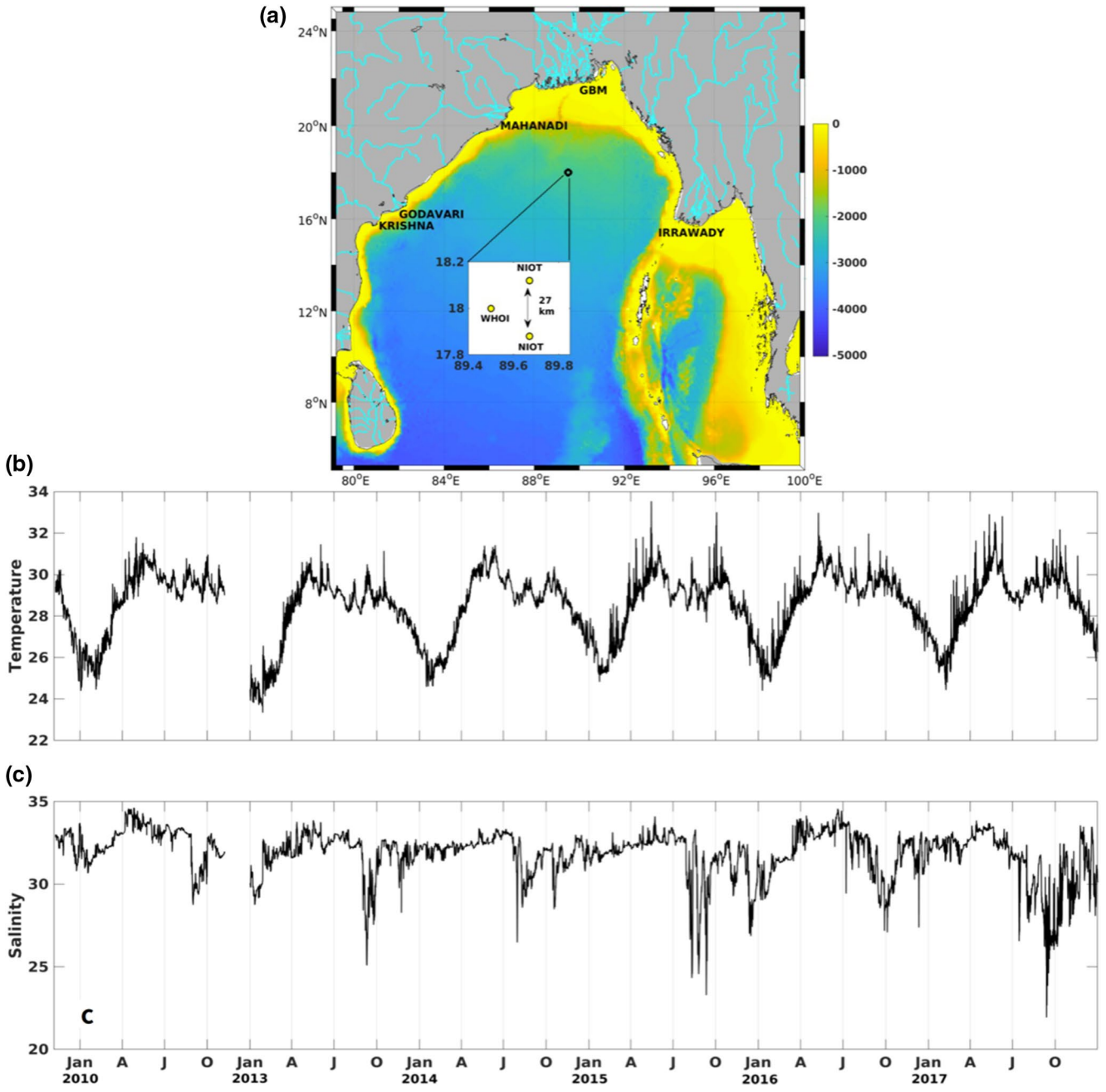

Figure 1. (a) Bay of Bengal bathymetry from ETPO2 (color; m); Ganga-Brahmaputra-Meghna (GBM), Irrawady, Mahanadi and other major rivers (cyan), and locations of the 18°N INCOIS/WHOI and NIOT moorings (inset). Hourly time series of (b) surface temperature (°C) and (c) surface salinity (psu) from the INCOIS mooring (18°N, 89.5°E), WHOI mooring (18.01°N, 89.45°E) and NIOT mooring BD08 (18.12°N, 89.67°E). The record extends from November 2009 to November 2010, and January 2013 to December 2017. The shallowest depth at which measurements are available is 1 m in 2010, 2013, and 2015; 4 m in 2014, and 5 m in 2016–2017. A mooring deployed in 2011–2012 was lost.

arrival of low-salinity water from the GBM river at the mooring (Figure 1c; Sengupta et al., 2016; Sree Lekha et al., 2018). Recent modeling and observational studies indicate that the low values of salinity observed in December–February have their origin in the Andaman Sea, in particular Irrawady river runoff (Benshila et al., 2014; Gordon et al., 2016; Sengupta et al., 2016; Shroyer et al., 2020). Surface salinity does not exceed 35 psu at any time, but is relatively high during March–May. At this time of the year, saltier water from the southern bay is carried to the mooring by a swift western boundary current that leaves the coast and flows eastward to the open ocean at 17–18°N latitudes (Gangopadhayay et al., 2013).

The moored observations show significant year-to-year changes in surface salinity. For example, the lowest salinities in 2010 (28 psu) and 2017 (22 psu) differ by ∼6 psu; the pulse of low-salinity water (salinity less than 29 psu) persists at the mooring location for the entire month of September in 2017, considerably longer than in other years. Interannual changes in BoB surface salinity arise mainly from year-to-year differences in rainfall minus evaporation, the pathways of river runoff in the open ocean, and rates of export through the open southern boundary of the BoB (Akhil et al., 2016; Durand et al., 2013). Energetic, long-lived mesoscale eddies (eddy lifetimes of several months and eddy diameter 200–400 km) are an important part of intraseasonal to seasonal-scale circulation in the northwestern BoB. Year-to-year differences in the eddy field can influence the pathways of GBM river runoff in the northern bay (Fournier et al., 2017; Kumar et al., 2013). Pant et al. (2015) and Chaitanya et al. (2015) show from models and observations, that interannual variability of basin-scale SSS in the BoB arises from differences in large-scale circulation associated with positive/negative phases of the Indian Ocean Dipole mode (Saji et al., 1999; Webster et al., 1999).

A fourteen-month long record of moored measurements at the WHOI mooring (Weller et al., 2019) show distinct episodes when surface salinity abruptly falls by 3–8 psu in August–September and November–December 2015, upon arrival of fresh water at the mooring (Figure 2a). The maximum vertical gradient in salinity in the upper 10 m is 7 psu during these episodes. Precipitation (P) peaks in the summer (or southwest) monsoon season; the highest rainfall measured at the mooring exceeds 150 mm/day during the passage of tropical storm Komen in late July–early August. Mean evaporation (E) is 3–4 mm/day during spring and summer, and highest (5–6 mm/day) during the winter months (Figure 2b) because the air is dry and cool. Although surface fresh water flux ($P - E$) at the mooring has energetic subseasonal variability, there is no one-to-one relation with the low salinity events.

To set the stage for study of sub-seasonal variability of surface salinity in the BoB, we used WHOI mooring observations to estimate the freshwater content (Carmack et al., 2008; Sengupta et al., 2006; Steele et al., 1996) in the upper 10 m using: $FWC = \int_{-10}^{0}\left[1 - \frac{S(z)}{S_o}\right]dz$, where $S(z)$ is the measured salinity as function of depth z, S_o is reference salinity, taken as 35 psu. The freshwater content represents the amount of pure freshwater (in meters) which would have to be mixed with 35 psu water to match the observed depth-integrated salinity.

The freshwater balance in the upper 10 m of the ocean constructed from surface evaporation, rainfall, and salinity data at the WHOI mooring suggests that the abrupt 3–8 psu drops in salinity in August–September 2015 cannot arise from the effect of local rainfall (Figure 2c). Freshwater content in the upper 10 m shows a gradual decrease during January–June, in keeping with the cumulative effect of net freshwater loss from the ocean surface. During the passage of tropical storm Komen (25 July to 2 August 2015), freshwater content rises by 0.5 m in 4 days due to local precipitation. We show later that the three distinct pulses of freshwater content, with amplitudes of 1.2–2 m in August–September, are due to lateral advection of GBM river water. In November–December, arrival of low-salinity water from the Andaman Sea leads to increase of freshwater content by 0.5–1 m (Sree Lekha et al., 2018).

3.1. Quasi-Biweekly Variability in Surface Salinity and Winds

Figure 3 shows variance preserving spectra of daily surface temperature, salinity and wind speed from the mooring time series, and of daily GBM river discharge. The spectra estimated for individual years is

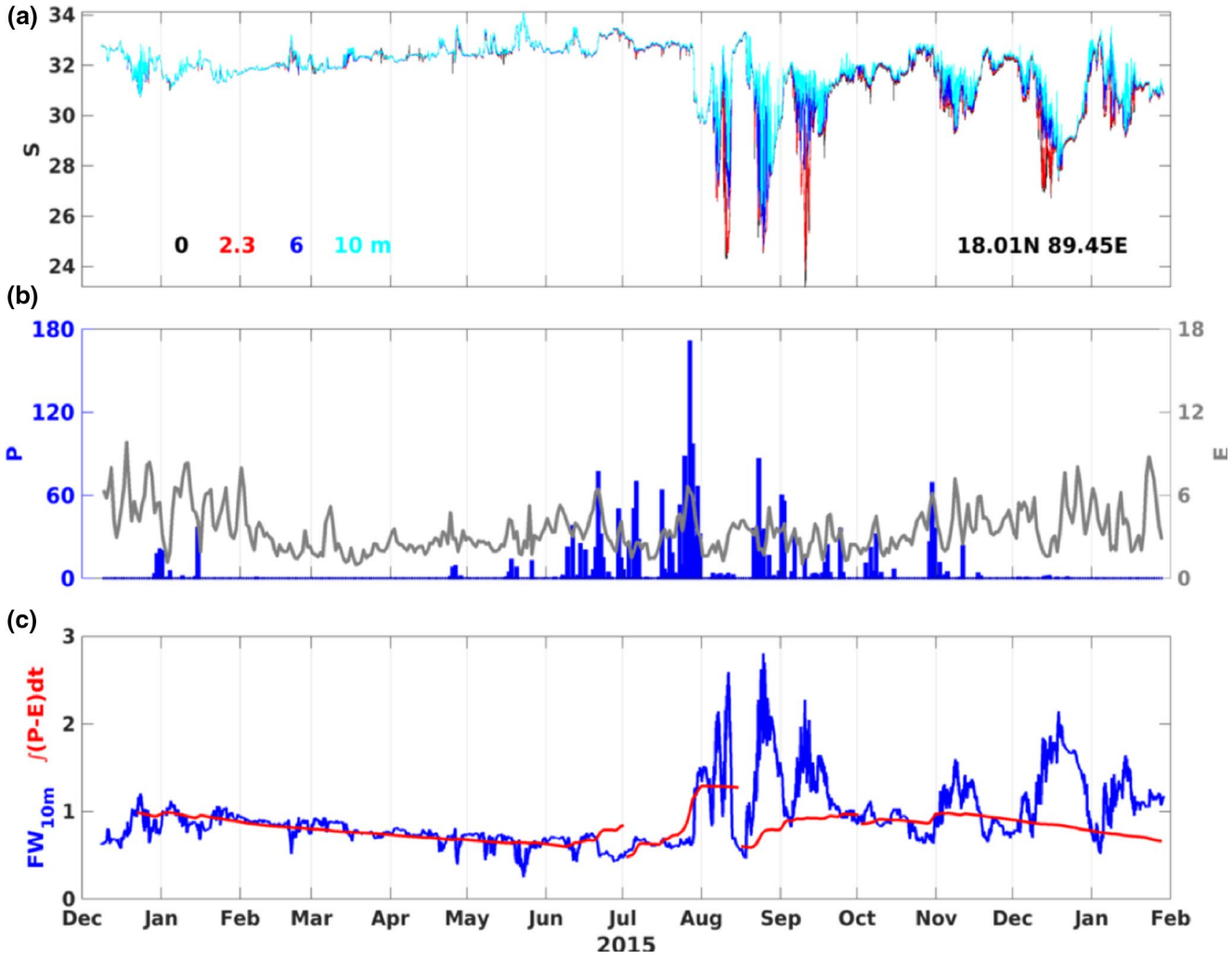

Figure 2. (a) Hourly salinity (psu) at 0, 2.3, 6, and 10 m from the WHOI mooring (18.01°N, 89.45°E). (b) Daily TropFlux evaporation (right axis; gray, mm/day) and daily TRMM 3B42v7 rainfall (left axis; blue bars, mm/day) at the mooring location. (c) Fresh water content in the upper 10 m (left axis; blue, m); time integral of surface fresh water flux P-E (red, m), in three stretches starting December 20, 2014, July 1, 2015, and October 1, 2015.

shown in thin gray lines; the average of the spectra from the six individual years is in bold (Figure 3a). The SST spectra show dominant variance at 40–60 and 10–20 day timescales, in line with previous studies (e.g., Goswami, 2012; Han et al., 2006; Parekh et al., 2004; Sengupta & Ravichandran, 2001; Vecchi & Harrison, 2002). The spectra of surface salinity and wind speed, on the other hand, show a distinct peak at the quasi-biweekly period (Figures 3b and 3c; Goswami, 2012, Subrahmanyam et al., 2018, Prend et al., 2019, Roman-Stork et al., 2019, Paul & Sukhatme, 2020). River discharge is a major source of low-salinity water in the open ocean of the BoB, as discussed earlier. The power spectrum of 18 years (1995–2013) of daily GBM river discharge shows a broad peak at 30–60 day period (Figure 3d). There is little or no variance at 10–25 day period except in 1 year, 2004, when the *in situ* gauge measurements in Bangladesh are unreliable. The spectra indicate that the observed quasi-biweekly variability of moored SSS cannot be attributed to variations in river discharge.

Both surface salinity and surface temperature measured at the moorings have significant ISV (Figures 4a–4l). Mean variance preserving SST spectra estimated from daily mooring observations in May–October over six years show distinct peaks at 20–40 and 10–20 day periods; the quasi-biweekly band contains nearly one-third of the total 10–60 day variance (Figure 4m).

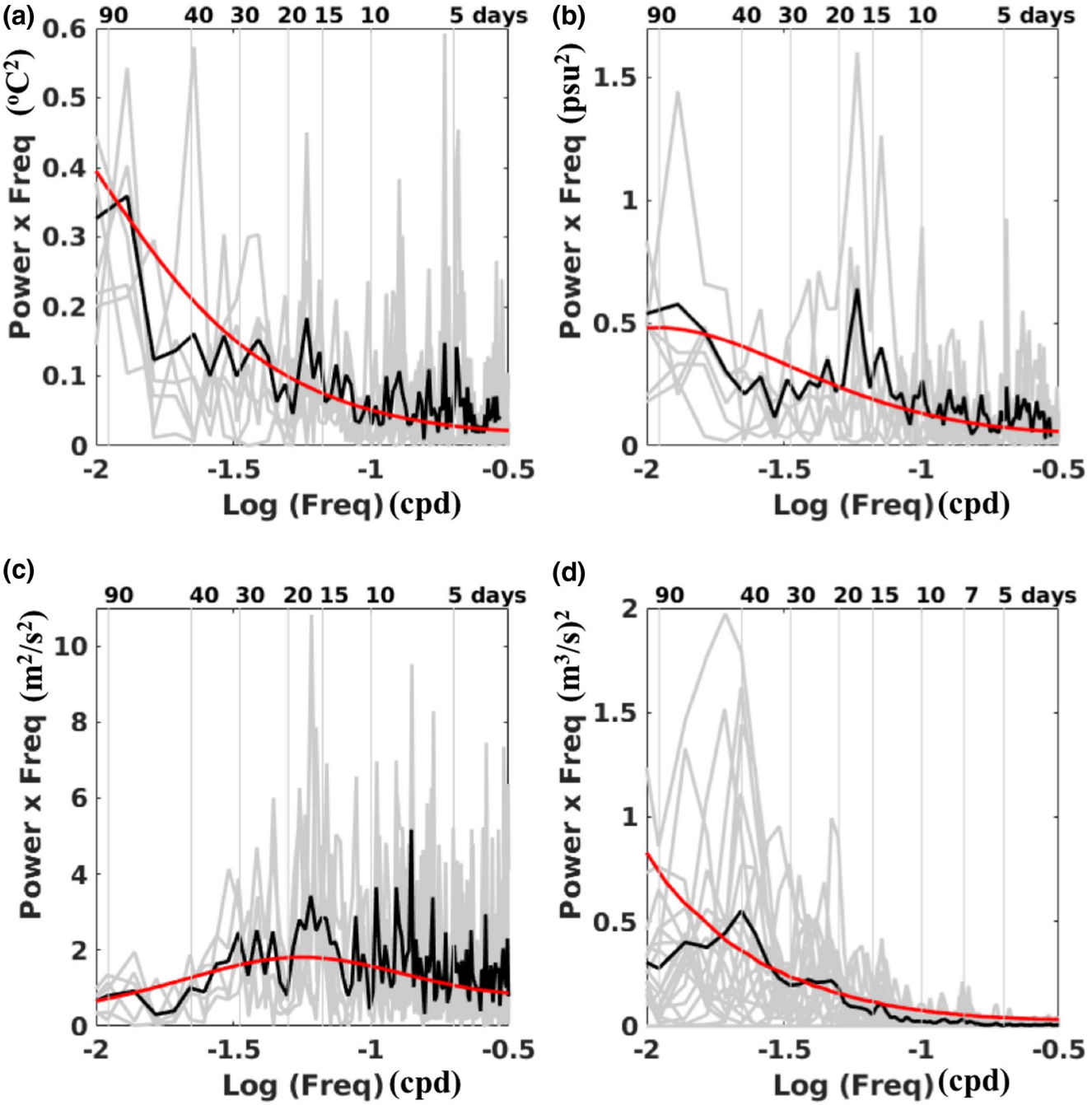

Figure 3. Variance preserving spectra of daily moored observations of (a and b) surface temperature and surface salinity (6 years 2010, 2013–2017), (c) wind speed (5 years, June 2011–June 2014 and June 2015–June 2017) and (d) Ganga-Brahmaputra-Meghna river discharge (18 years, January 1995–December 2013). Spectra computed using 1 year-long time series is shown in gray; the black line represents the average of the spectra for individual years and the 99% significance curve (red) is shown. The depth of temperature and salinity sensors is the same as in Figure 1. Units on *x* axis is cycles per day (cpd). In variance-preserving form, the area under the spectral curve between two frequencies is proportional to variance in that frequency band.

In summer, ISV of SST (or mixed layer temperature) in the north BoB is mainly a response to net heat input to the mixed layer: $hC_p\rho\frac{\partial SST}{\partial t} = Q_{net} - Q_{pen}$, that is, $SST(t) = \int_0^t \frac{Q_{net} - Q_{pen}}{\rho C_p h} dt$, where Q_{net} is net surface heat flux, and Q_{pen} is the penetrative flux of shortwave radiation below the mixed layer (Sengupta & Ravichandran, 2001). Q_{pen} at depth z can be estimated from: $Q_{pen}(z) = Q_{SW}\mathrm{Re}^{\frac{-z}{\zeta 1}} + Q_{SW}(1-R)e^{\frac{-z}{\zeta 2}}$, where

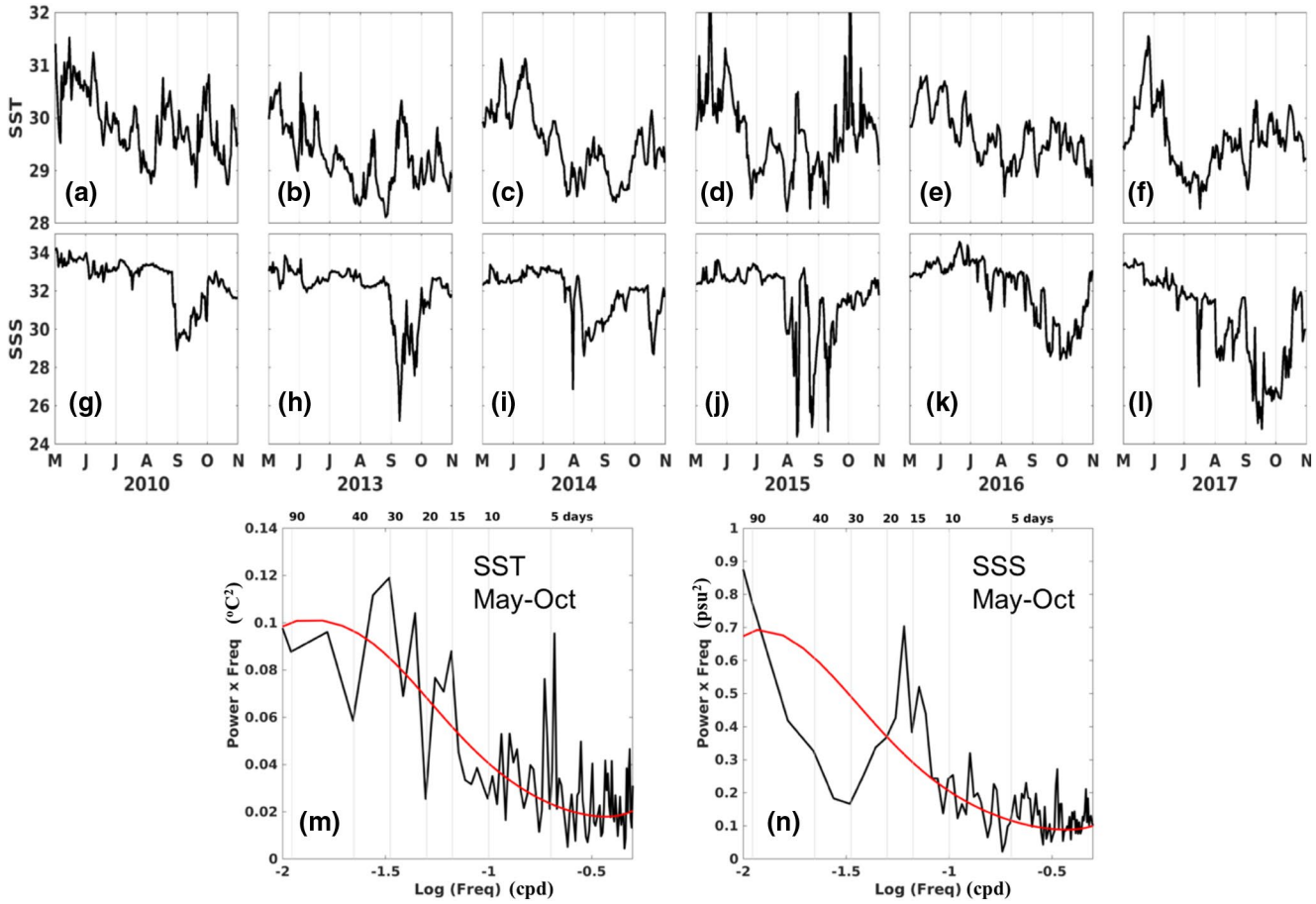

Figure 4. (a–f) Daily surface temperature (T) and (g–l) daily surface salinity (S) from the 18°N, 89.5°E moorings during May–October of 2010 and 2013–2017. The depth of T and S measurements is the same as in Figures 2b and 2c. (m and n) Mean variance preserving spectra of daily T and S in May–October, averaged over the six years of moored observations. The 99% significance curve (red) is shown in panels (m) and (n).

Q_{SW} is the net (incident minus reflected) surface flux of shortwave radiation, $R = 0.62$, ζ_1 and ζ_2 are the attenuation depths, taken as 1.5 and 20 m respectively (Paulson & Simpson, 1977), h is mixed layer depth, C_p is the specific heat, ρ is density of sea water and t is time. Since SST effectively responds to the time integral of heat input to the mixed layer, the SST response to heat flux having broad-band variability is preferentially at lower frequencies. Duncan and Han (2009) have shown from satellite microwave SST and HYCOM ocean model simulations, that the peak SST response in the northwestern Bay is at 30–90 days, although net surface heat flux has highest variance at 10–30 day scale. Unlike SST, the mean variance preserving spectrum of May–October surface salinity (Figure 4n) has a peak at 10–30 days. In the following sections, we study the physical mechanisms that give rise to the quasi-biweekly variability of salinity observed at the moorings.

4. Observed Quasi-Biweekly Variability in the 2015 Summer Monsoon Season

In this section, we present results on the quasi-biweekly atmospheric mode, and relate it to the space-time variability of near-surface salinity in the BoB during the summer of 2015.

4.1. Large-Scale Variability of Rainfall and Winds in the Northern Tropics

We begin with the large-scale, westward propagating quasi-biweekly oscillations of 2015 summer monsoon rainfall and winds in the tropical Pacific and Indian Ocean, as seen in satellite rainfall and reanalysis winds.

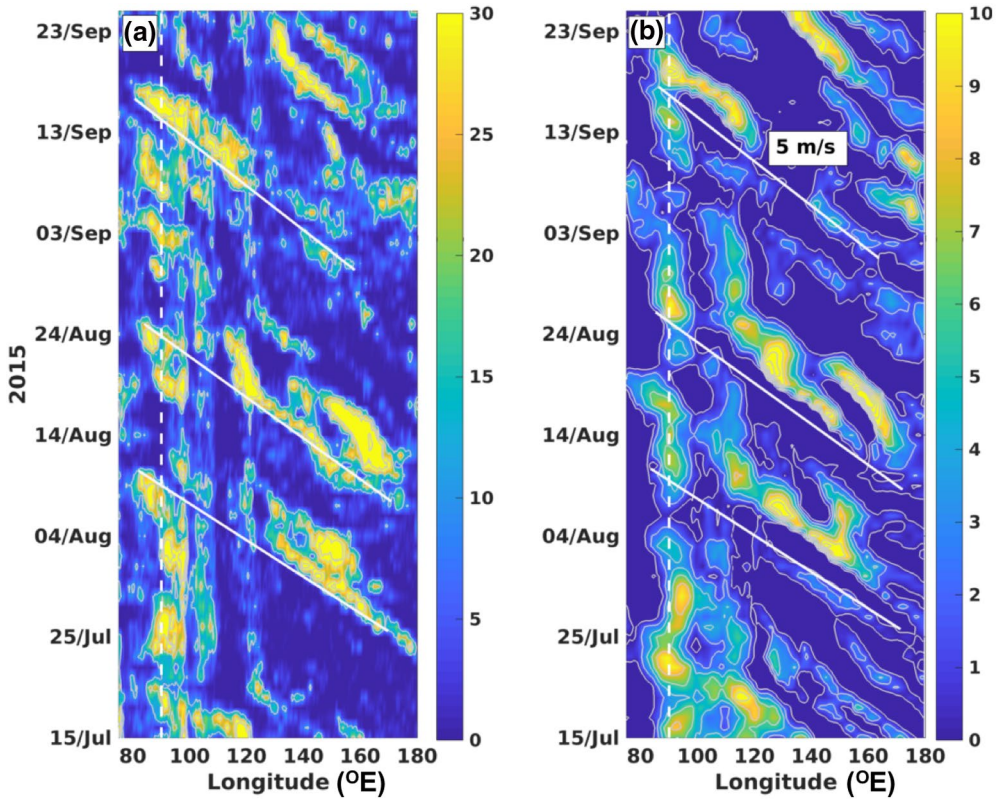

Figure 5. Hovmoller (longitude-time diagrams) over 15 July to 30 September 2015 of (a) daily TRMM 3B42v7 rainfall (mm/day) and (b) daily MERRA2 850 hPa meridional wind V_{850} (m/s), both averaged over 10°N–16°N latitude; only northward V_{850} (positive values) are shown in color and contours. The dotted line is at 90°E in the mid-Bay of Bengal. Westward propagation speed is estimated from the slope of the white lines, which are identical in the two panels.

We construct longitude-time plots (Hovmoller diagrams) of unfiltered daily TRMM3B42 V7 rainfall and daily meridional wind at 850 hPa (V_{850}) from MERRA2 reanalysis during July–September 2015; both quantities are averaged over 10°N–16°N (Figure 5). The observations show periods of heavy rainfall (20–30 mm/day), closely followed by strengthened northward V_{850} (up to 8–10 m/s). The enhanced rainfall and V_{850} signals originate near the dateline and propagate westward at 4–5 m/s across the west Pacific Ocean, into the BoB and the Indian subcontinent; the intervals between successive episodes of enhanced rainfall and wind (marked by the sloping lines on Figure 5) are about 12–14 and 20–22 days. Two other westward moving signals, in July (140°E–80°E) and September (180°E–140°E), have similar propagation speed. Thus, the large-scale convective episodes have a recurrence time of 2–3 weeks in the summer of 2015, a clear manifestation of the quasi-biweekly mode of the Asian monsoon (Chen & Chen, 1993; Krishnamurti et al., 1985).

We illustrate the space–time evolution of the quasi-biweekly monsoon mode using a sequence of daily rainfall and 850 hPa wind maps during the September 2015 episode (Figure 6). A 10°-wide westerly zonal jet spans over 10,000 km (70°E–170°E) on September 10, 2015, associated with a zonal band of rainfall (Figure 6a). The core of the jet lies near 5°N in the Pacific and 10°N in the north Indian Ocean; in the independent TRMM dataset, the heaviest rainfall (60–100 mm/day) is also seen to lie around these latitudes. A double-vortex structure characteristic of the equatorially-trapped first meridional mode Rossby wave is seen in the Pacific at 140°E–170°E, and also discernible in the eastern Indian Ocean (e.g., the review of Goswami, 2012). The zonal jet at 850 hPa appears to be unstable—on 12 September, two prominent synoptic-scale (1,000–1,500 km diameter) cyclonic vortices lie on the northern flank, one around 90°E and another at 115°E (Figure 6b). By 14 September, the BoB vortex has intensified to a monsoon low-pressure system, while the eastern vortex has grown in size and intensity over the South China Sea and adjoining land (Figure 6c). During the next four days, the BoB system moves across central India as a deep depression (India Meteorological Department; IMD Monsoon Re-

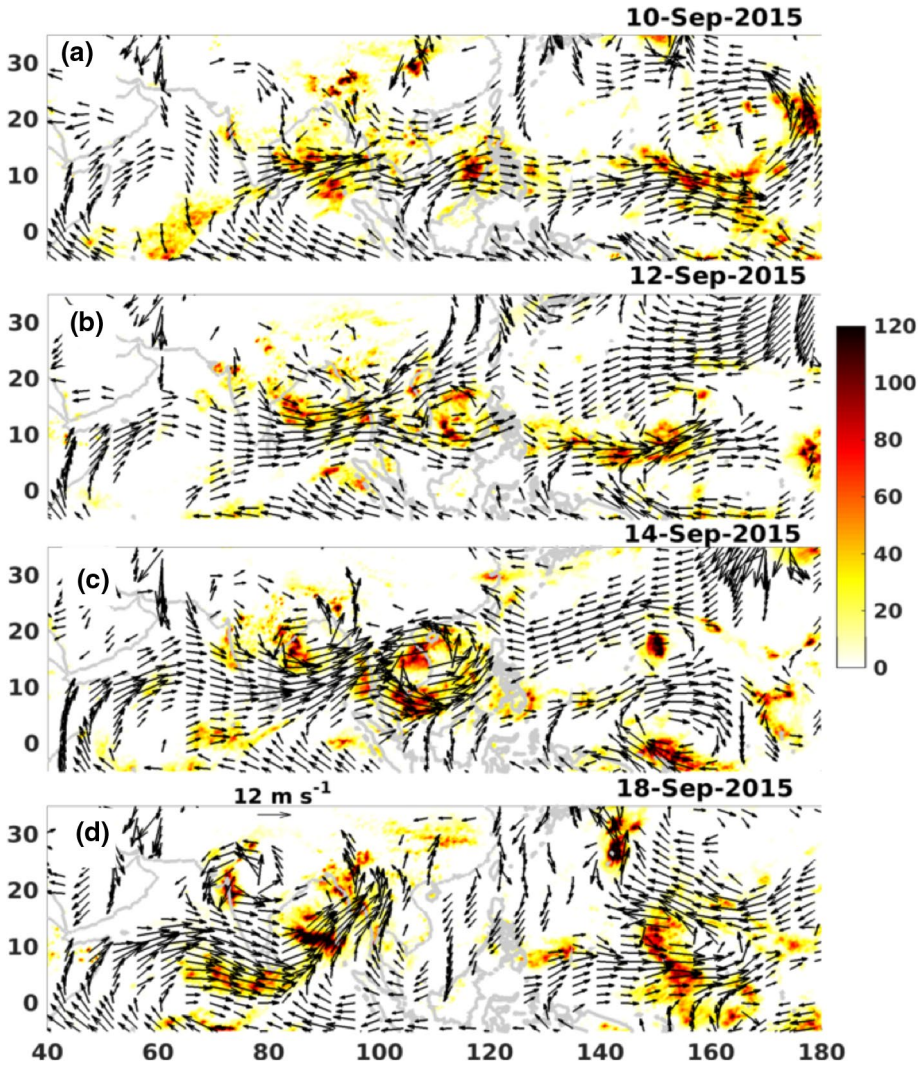

Figure 6. Daily TRMM 3B42v7 rainfall (mm/day; color) and MERRA2 850 hPa winds (m/s; vectors) on selected days: 10, 12, 14, and 18 September 2015. Wind vectors with magnitude less than 5 m/s are not shown. A 12 m/s reference vector is shown in bottom panel.

port, 2015), bringing widespread rainfall to the region. Meanwhile, the eastern cyclonic system moves from the South China Sea into the BoB, where the southwesterly wind speed at 850 hPa reaches 18 m/s on 18–19 September (Figure 6d).

The evolution of rainfall and winds associated with the quasi-biweekly oscillation in July–August 2015 (see Figure 5) has basic characteristics in common with the September episode: Synoptic-scale cyclonic systems are embedded in the northern flank of the meandering, westerly monsoon flow in the east Indian Ocean and west Pacific Ocean sectors. To its north, the westerly low-level monsoon jet (Joseph & Sijikumar, 2004) is associated with large-scale cyclonic vorticity, favoring genesis of monsoon low-pressure systems and depressions in the BoB (Goswami et al. 2003). The large-scale westerly flow sometimes extends east of 140°E in July–August; unlike the September episode, the occasional weather system intensifies and moves northwestward rather than westward in the western north Pacific (not shown).

4.2. Quasi-Biweekly Variability of Salinity in the Summer of 2015

In July–September 2015, salinity measured at the 18°N WHOI mooring, SMAP SSS and surface salinity from the global ocean analysis all show three distinct low-salinity pulses, with 8-day running mean SSS

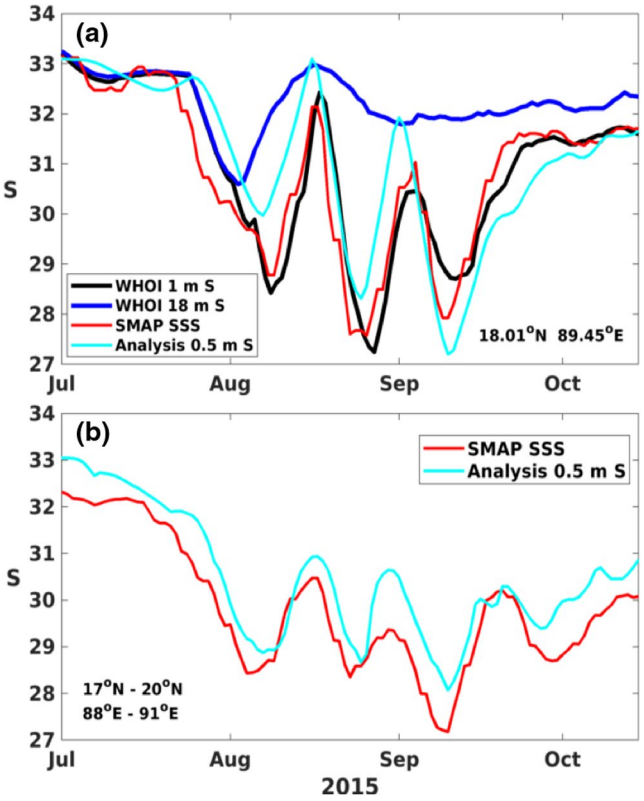

Figure 7. (a) Eight-day running mean salinity (psu) at 1 m (black) and 18 m (blue) depth from the WHOI mooring (18.01°N, 89.45°E) observations; SMAP gridded sea surface salinity (SSS; red), and salinity at 0.5 m depth from the ocean analysis (cyan) interpolated to the mooring location during 1 July to 10 October 2015. (b) SMAP SSS (psu; red) and salinity at 0.5 m depth from ocean analysis, spatially averaged over 17–20°N, 88–91°E, 1 July to 10 October 2015.

alternately falling and rising by 2–5 psu approximately every two weeks (Figure 7a). Analysis and satellite SSS in July–October 2015 closely follows the moored observations—the bias of SMAP SSS relative to mooring is 0.08 psu, and the bias of ocean analysis SSS is −0.17 psu. Surface salinity falls ("freshening") when water from the GBM river reaches the mooring (Sengupta et al., 2016), and rises ("salting") when river water recedes, as we show below. The 1–5 psu difference in salinity between 1 and 18 m depths at the WHOI mooring indicates very stable density stratification, as estimated from the Brunt-Vaisala frequency $N = \sqrt{\frac{-g}{\rho_o}\frac{d\rho}{dz}}$, where g is acceleration due to gravity, ρ_o is the mean potential density of sea water, and ρ is density at depth z. The maximum value of N estimated from mooring data is 1.8×10^{-2} s^{-1}; stratification is dominated by the vertical gradient of salinity rather than temperature. Mixed layer depth ranges from less than 1 m when SSS is low, to about 10 m when SSS is relatively high during these freshening and salting episodes (Prend et al., 2019). The observed drop in salinity at 18 m depth in late July could be due to low-salinity surface water mixed downwards by tropical storm Komen in the north BoB (IMD, 2015; Weller et al., 2019). The SSS variability on quasi-biweekly timescale at the mooring is part of larger-scale variability in the north bay (Figure 7b).

Maps of SMAP SSS and AVISO geostrophic surface current vectors during the three freshening and salting episodes show that SSS falls when low-salinity river water (dark blue shade, SSS less than 29 psu) is drawn to the mooring (Figures 8a, 8c, and 8e) by the flow (speed 0.3–0.5 m/s) between two counter-rotating mesoscale eddies, with centers at 16.5°N 90.5°E and 18.5°N 88°E, and diameters of about 200 km and 300 km. Surface salinity rises when river water moves away from the mooring (Figures 8b, 8d, and 8f). There is no major change in the flow between the two counter-rotating mesoscale eddies, other than a gradual weakening of the eastern eddy. A nearly basin-wide cyclonic gyre to the north of 18°N in early August (Figure 8a) gradually weakens and disappears by 10 September (Figure 8e). The patch of relatively high SSS at 20°N within the pool of river water (Figure 8a) is a remnant of wind-induced vertical mixing of the upper ocean by tropical storm Komen.

4.3. Surface Wind, Ocean Current, and Salinity

The three episodes of alternate freshening and salting observed at the WHOI mooring are directly related to changes in surface winds in August and September: Surface salinity falls as the surface wind speed decreases, and salinity rises when surface wind speed increases (Figure 9a). The average wind speed at the three moorings is 2–4 m/s when surface salinity is lowest and 7–10 m/s when surface salinity is high. Figures 9b–9d shows measured wind vectors, and ocean current vectors during periods of freshening at the 18°N moorings. When the northward component of surface wind is weak, stirring by mesoscale eddies draws river water to the mooring, leading to freshening. At these times, moored surface currents are generally comparable to AVISO surface geostrophic currents in magnitude and direction. During 8–11 September (Figure 9d), the moorings are located in a region with very weak surface and subsurface currents, just outside two mesoscale eddies (see Figure S1). During episodes of increasing surface salinity ("salting"), the northward component of wind is strong and a shallow, directly wind-forced Ekman current (estimated from moored surface velocity minus 60 m velocity) with speeds of upto 0.4–0.5 m/s (Figures 9e–9g) disperses river water to the north and east, away from the moorings (Figures 8b, 8d, and 8f). During the individual episodes of freshening and salting, subsurface (60 m) currents associated with mesoscale eddies do not change significantly in August, but weaken in September (Figures 9b–9g).

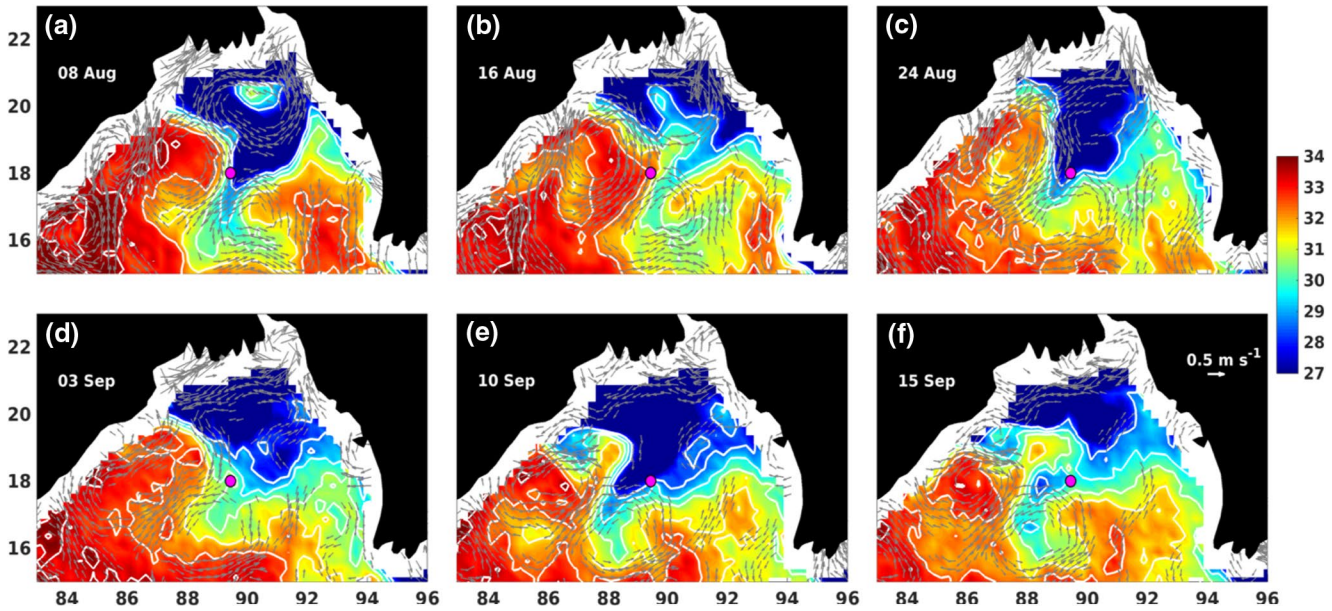

Figure 8. (a–f) SMAP SSS (psu; color and contours) and AVISO geostrophic ocean current vectors on selected days during the three freshening and salting periods in summer 2015. The WHOI mooring is marked by a pink dot; 29, 30, and 31 psu SSS contours are in white; dates are in top left of each panel; a reference current vector is in panel (f). Current vectors with magnitude less than 0.1 m/s are not shown.

The observed changes in surface salinity at the moorings as well as in SMAP SSS are mainly due to lateral advection by time-varying shallow ocean currents in the presence of large lateral gradients of surface salinity. The area covered by river water (salinity less than 29 psu) rises and falls in response to quasi-biweekly variations of surface currents driven by wind stress (Figure 8), explaining the variations in area-averaged SSS tendency in a somewhat larger region enclosing the moorings (Figure 7b). The three-dimensional salinity field from the ocean analysis indicates that the total volume of low-salinity water does not change on quasi-biweekly scales (see Fgure S2). It is nevertheless possible that a part of the salinity variability is due to mixing; but this question will be addressed in a future study.

Thus, the observations show that during active (rainy and windy) phases of the summer monsoon, shallow ocean currents forced by the northward component of surface wind stress carries river water to the north and east. When the monsoon is in a quiescent (dry and calm) phase, the river water is carried back towards the open ocean by the geostrophic flow. This basic mechanism explains the quasi-biweekly fluctuations in area-averaged SSS in the north BoB (Figure 7b). We note that lateral and vertical mixing may play a role in the evolution of the salinity field, but the effects of mixing do not appear to be dominant on the quasi-biweekly scale in the summer of 2015 (Figure S2). Sree Lekha et al. (2018) discuss the role of mesoscale eddies and directly wind-forced ocean currents in the dispersal of river water during the 2013 summer monsoon season. Unlike 2015, Ekman currents led to a fall in SSS in the open ocean (central longitudes) rather than a rise, since the main pool of river water lay in the northwestern BoB in summer 2013. As in the summer of 2013, river water reaches the interior from the northwestern boundary of the bay in 2017, due to eddy stirring as well as Ekman flow. The quasi-biweekly variability of SSS is not prominent in 2017, since the mooring lies well within the pool of river water from 10 September to 15 October, and the boundary between the river water and saltier ocean water is not advected past the mooring (Figure 4l).

4.4. Relation Between Surface Winds and Sea Level

Daily sea level from the global ocean analysis at Chittagong station, located at 22.27°N, 91.81°E is in good agreement with daily *in situ* tide gauge data (Figure 10a). During August–September 2015, sea level at

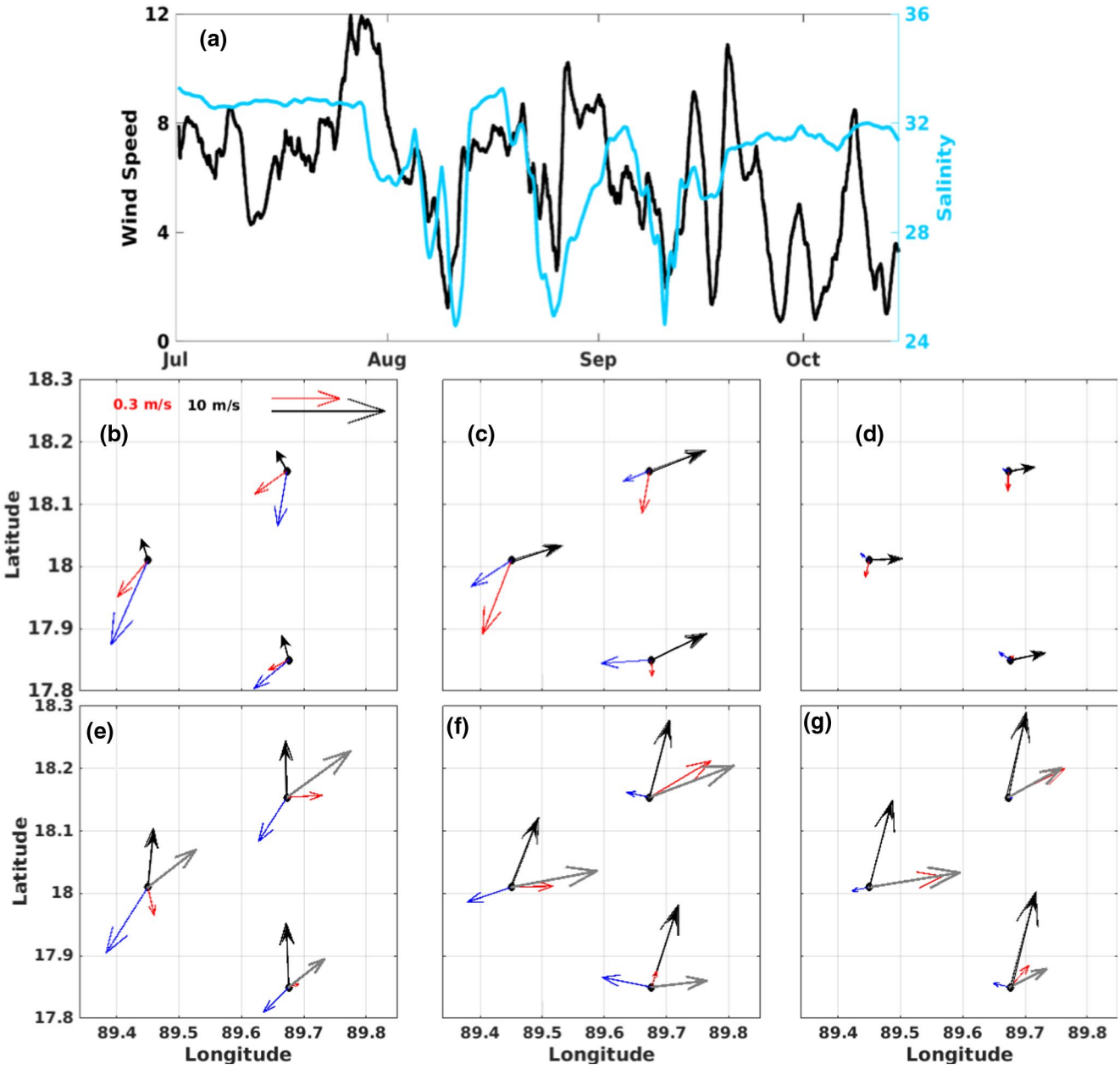

Figure 9. (a) Daily salinity at 1 m (blue) and surface wind speed (black) measured at 3.47 m and adjusted to 10 m height at the WHOI mooring (18.01°N, 89.45°E) during July–October 2015. Surface wind vectors (black), ocean surface currents (red) and 60 m currents (blue) at the WHOI mooring and nearby NIOT moorings BD09 (17.88°N, 89.67°E) and BD08 (18.15°N, 89.67°E), averaged over two inertial periods (i.e., 80 h), during the (b–d) freshening and (e–g) salting events. The averaging dates are (b) 7–10 August, (c) 21–24 August, (d) 8–11 September in the freshening spells; and (e) 11–14 August, (f) 25–28 August, and (g) 13–16 September in the salting spells. The Ekman current, obtained by subtracting the current at 60 m depth from the surface current, is shown as gray vectors in panels (e–g). Reference wind vector (7 m/s, black) and current vector (0.3 m/s, red) marked in panel (b).

Chittagong shows a remarkably clear variability on quasi-biweekly timescale. The *in situ* sea level data has been de-tided, and the global ocean analysis does not include tides in the model configuration, so we rule out a possible relation to the spring-neap cycle. The magnitude of surface wind stress from daily MERRA2 reanalysis, averaged over the BoB north of 17°N latitude, has a clear relation with sea level: high (low) wind stress is associated with high (low) sea level, and the two quantities vary nearly in phase (Figure 10b). Composite maps of 2-day average sea level from global ocean analysis during low-wind and high-wind events are shown in Figures 11a and 11b.

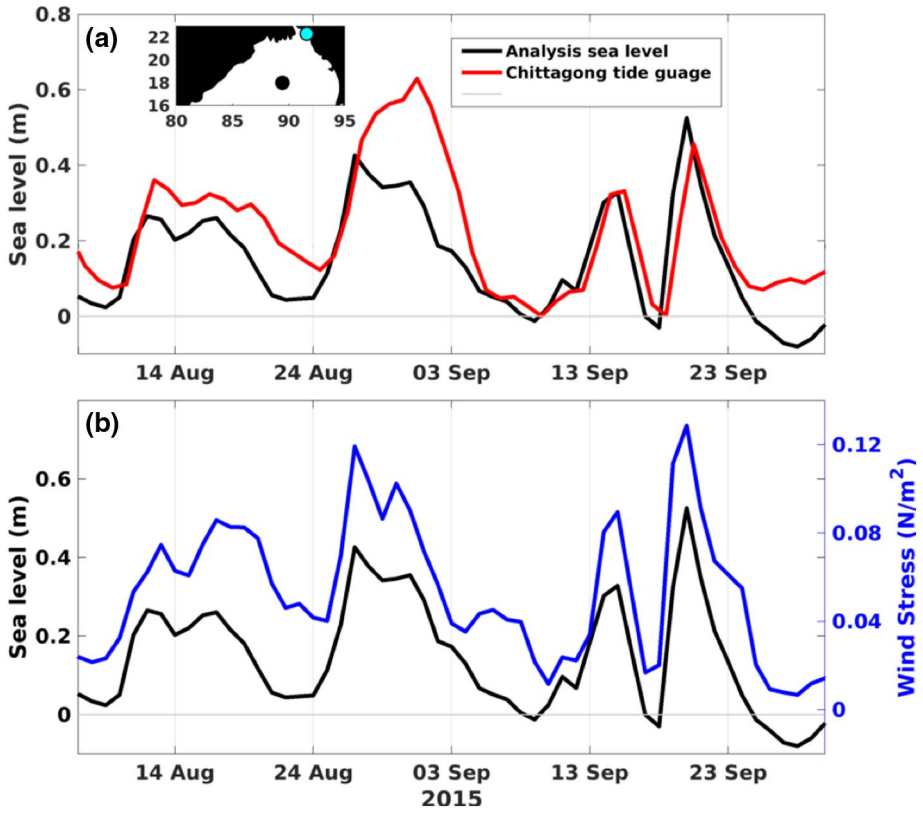

Figure 10. (a) Daily sea level anomaly from global ocean analysis (m; black) and tide gauge measurements (m; red) at Chittagong (22.27°N, 91.81°E), 1 August to 30 September 2015. The locations of the Chittagong tide gauge (cyan) and WHOI mooring (black) are shown in inset. (b) Daily sea level anomaly from global ocean analysis (m; black), and magnitude of MERRA-2 surface wind stress (N/m^2; blue, right axis) averaged over the oceanic region north of 17°N, 1 August to 30 September 2015.

The mean magnitude of surface wind stress averaged over the oceanic region north of 17°N is about 0.05 N/m^2 during low wind episodes, and 0.3 N/m^2 during high wind episodes. Within two days of high surface winds, sea level at the eastern boundary of the BoB rises by at least 0.1 m; along the northern boundary of the bay, composite sea level rises by 0.2–0.3 m. When the southwesterly monsoon winds strengthen, an "Ekman" flow (nearly 0.4 m/s in magnitude) in the upper 15 m disperses the low-salinity river water toward the northern and eastern boundary of the bay, raising sea level within 100–200 km of the coast (see Figrue S3). The daily ocean analysis data shows a downwelling Kelvin wave, propagating at about 2 m/s with the coast to its right, reaching the western boundary of the bay (the east coast of India) in about 2 days. We attempted to track the Kelvin wave further in but could not discern a clear signature south of 18°N on the western boundary.

5. Heat Fluxes and SST Response in the Presence of Fresh Water

SMAP and analysis data show that low-salinity river water is confined to the northeastern BoB in early August to early September 2015, due to a persistent anticyclonic eddy and poleward geostrophic flow in the northwestern bay (Figure 8a). A sharp boundary separates the river water from saltier water in the northwestern bay (Figures 8 and 13a).

In order to examine the relation between surface salinity and SST evolution, we consider a sub-seasonal SST oscillation observed at the WHOI mooring in July–August 2015 (Figure 12a). Following the one-dimensional heat balance equation discussed in Section 3.1 (Sengupta & Ravichandran, 2001), we analyze the response of SST to net surface heat flux (Q_{net}) minus penetrative flux (Q_{pen}) of shortwave radiation below the

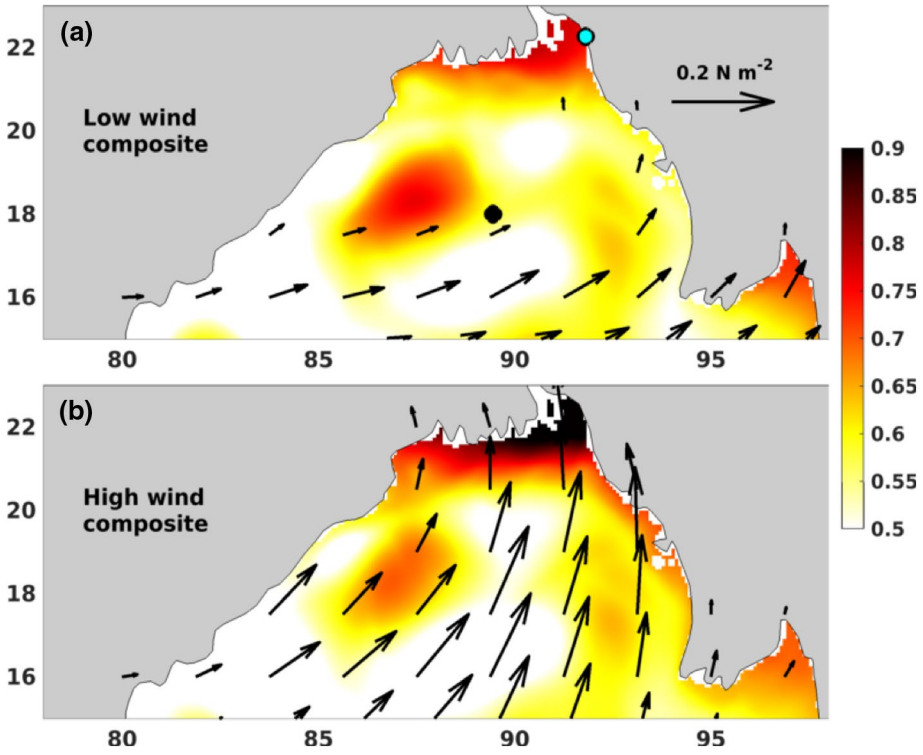

Figure 11. Composite of daily sea level from global ocean analysis (color; m) and daily surface wind stress from MERRA-2 atmospheric reanalysis (vectors; N/m^2) during (a) weak wind episodes (9 August, 23 August, 10 September) and (b) high wind episodes (13 August, 29 August, 19 September). The sea level in each episode is a 2-day average following the low and high wind dates. A wind stress reference vector, Chittagong tide gauge (cyan) and WHOI mooring (black) are shown in (a); wind stress less than 0.01 N/m^2 in magnitude is not plotted.

mixed layer. To estimate Q_{pen}, we use the Paulson and Simpson (1977) relation, with a specified minimum mixed layer depth of 5 m. The heat balance from moored observations suggests that the evolution of surface temperature is mainly a response to the net heat input to the mixed layer (Figure 12b). Next, we construct a similar one-dimensional heat balance in two 1° × 1° boxes, one inside the pool of river water (box 1), and another box outside the fresh pool (box 2; Figure 13a). Average SMAP salinity within the fresh pool remains below 30 psu from 20 July to 20 August 2015, with a minimum value of 25 psu; in contrast, SSS in the western box is in the range 31.8–33.8 psu (Figure 13b).

The multi-satellite microwave-based daily 0.25° OI SST dataset agrees with SST measured at the WHOI mooring, except during heavy rainfall (Figure S4; Gentemann et al., 2004). We estimate the bias in OI SST relative to the mooring and apply a bias correction to SST in box 1 (but not box 2). SST has a distinct 20-day oscillation in box 1, and relatively modest changes in box 2. The magnitudes of SST cooling and warming in box 1 are nearly 1°C in 7 days and 2°C in 9 days—the rate of SST cooling and warming are considerably higher within the fresh pool than in the saltier region to the west (Figure 13c). Note that average TRMM rainfall is comparable over the two boxes (Figure 13d); heavy rainfall exceeding 100 mm/day in the last week of July is associated with tropical storm Komen (Weller et al., 2019).

The mixed layer depth (MLD) used to estimate the flux of shortwave radiation below the mixed layer Q_{pen} is obtained from a regression between SSS and MLD from the WHOI mooring observations (Figure S5). Both net surface heat flux (not shown) and effective heat flux have distinct quasi-biweekly variability (Figure 13e), with the ocean losing heat in the cloudy, windy phase of the monsoon and gaining heat in the clear, calm phase. Although the amplitude of Q_{eff} variation in the salty region (−100 Wm^{-2} to +100 Wm^{-2}) is significantly larger than Q_{eff} variation inside the fresh pool, the rate of change of SST is higher in the presence of low-salinity surface water (Figures 13c and 13e). In other words, the presence of a thin, fresh layer of river water enhances SST response to heat flux on the quasi-biweekly timescale.

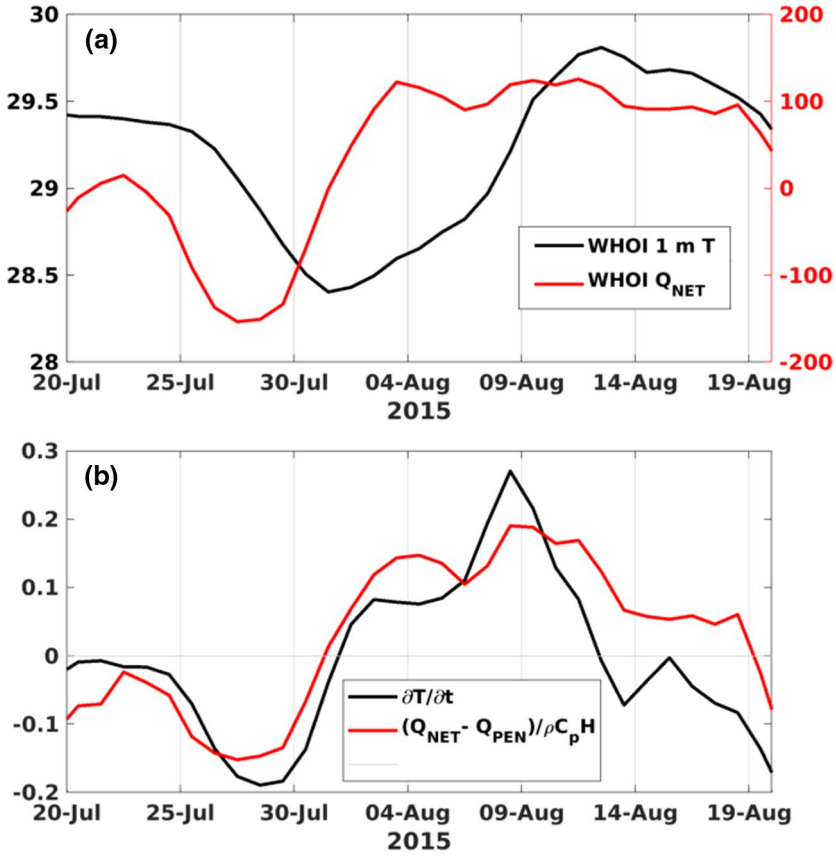

Figure 12. (a) Five-day running mean net heat flux (Q_{net}; W/m^2; red) and temperature at 1 m depth (°C; black) from **the WHOI mooring (18.**01°N, 89.45°E), 20 July to 20 August 2015. (b) Temperature tendency $\frac{\partial T}{\partial t}$ (°C/day; black) and forcing $\frac{Q_{net} - Q_{pen}}{\rho C_p h}$ (°C/day; red). Mixed layer depth h is defined as the depth where the potential density exceeds the 1 m density by 0.125 kg/m^3.

6. Summary and Conclusions

Six years of moored observations at 18°N, 89.5°E in the northern BoB, about 500 km away from the GBM and Irrawady river mouths, reveal distinct quasi-biweekly variability of near-surface salinity and surface winds during the southwest (or summer) monsoon season. Simple estimates based on freshwater balance indicate that the largest salinity changes (a few psu peak-to-peak) are not due to surface freshwater flux; nor are these changes due to subseasonal variation in freshwater discharge from the GBM river. Some of the highest amplitude quasi-biweekly salinity variations are seen in August–September 2015: Surface salinity measured at a cluster of three moorings rise and fall by 5–8 psu with nearly 15-day period. Sea surface salinity from the SMAP satellite and an ocean analysis dataset are in agreement with the *in situ* measurements. SMAP and analysis data show that river water lies in the northeastern BoB in the summer of 2015, and a sharp boundary separates it from saltier water in the northwestern bay. We find that during periods of calm surface winds, low-salinity water from the GBM river is carried to the moorings by geostrophic currents associated with mesoscale eddies, leading to a steep fall in surface salinity. When the southwesterly monsoon winds strengthen, surface salinity rises at the moorings.

The observed quasi-biweekly variability in the north BoB has its origin in the tropical Pacific Ocean near the dateline. Satellite rainfall and 850 hPa winds from reanalysis show coherent westward propagation of the quasi-biweekly summer monsoon mode and embedded synoptic systems, at a speed of nearly 5 m/s (Figure 5). Summer monsoon winds in the northern BoB strengthen in association with the 3,000 km-scale northern cyclonic vortex of the quasi-biweekly Rossby wave (Goswami, 2012). Surface wind stress is highest

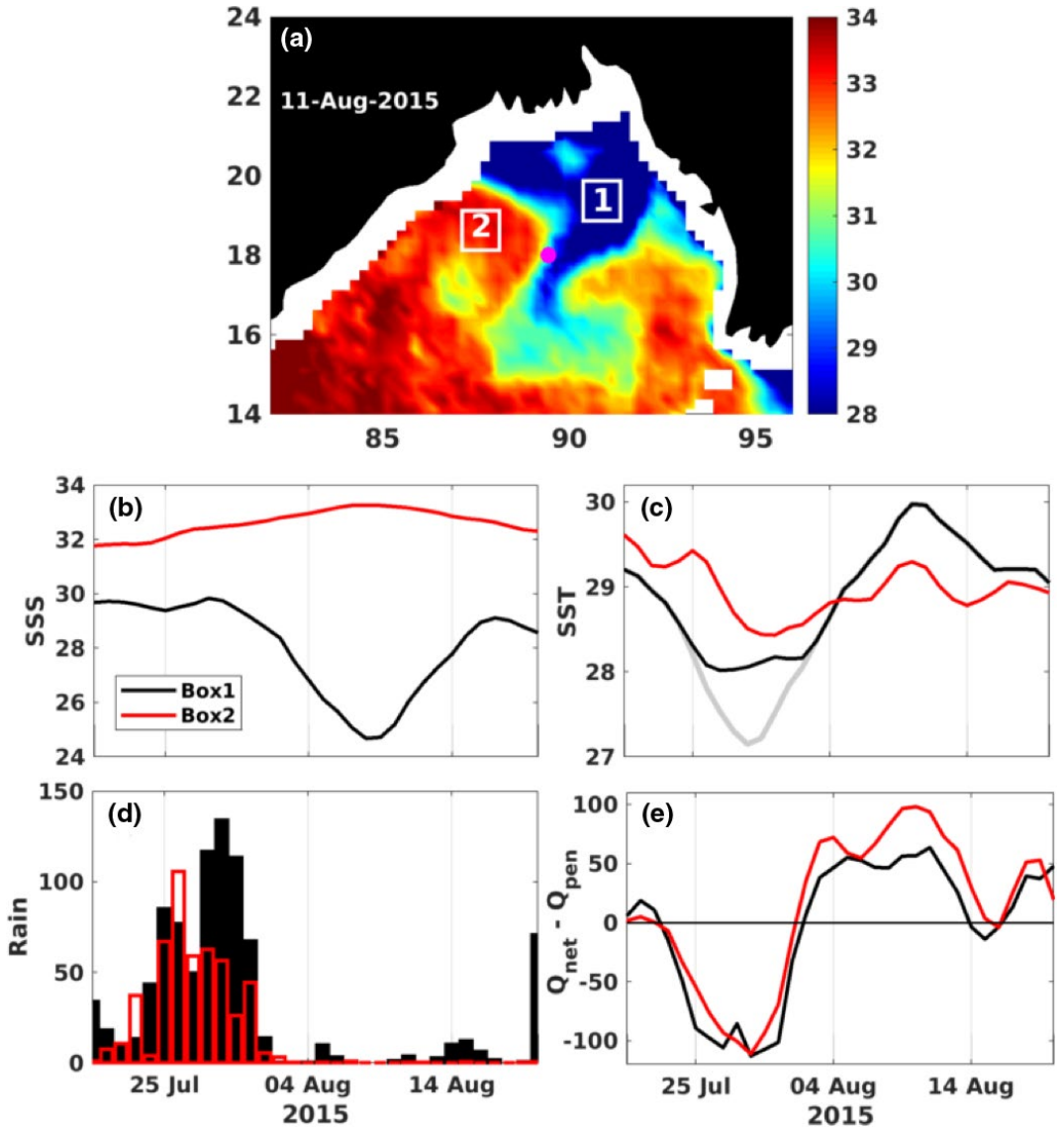

Figure 13. (a) Eight-day running mean SMAP SSS (psu; color) on August 11, 2015; two 1° × 1° boxes are marked—box 1 lies inside the pool of river water, and box 2 lies outside the low-salinity pool. (b) SMAP SSS (psu) and (c) Microwave OI daily sea surface temperature (SST; °C), averaged over box 1 (gray) and box 2 (red). The daily OISST averaged over box 1 is corrected for heavy rain-related bias (black) using WHOI mooring SST. (d) TRMM 3B42v7 daily rainfall (mm/day) averaged over box 1 (black bars) and box 2 (red bars). (e) Effective heat flux $Q_{net} - Q_{pen}$ (W/m^2), estimated from daily TropFlux surface flux data and daily mixed layer depth from ocean analysis (see text), averaged over box 1 (black) and box 2 (red).

when monsoon depressions (IMD Monsoon Report, 2015) intensify over the BoB, or when synoptic-scale cyclonic vortices move into the bay from the northwest Pacific Ocean and South China Sea. During active spells of the quasi-biweekly monsoon mode, a swift Ekman-like current (Sree Lekha et al., 2018) forced by enhanced northward wind stress disperses the shallow layer of river water to the north and east, raising sea level along the coast of Bangladesh and Myanmar by 0.1–0.5 m within 2–7 days (Figures 9–11). When surface winds weaken, the flow associated with mesoscale ocean eddies transports river water back toward the open ocean, and coastal sea level falls. Enhanced lateral gradients of steric height due to accumulation of low-salinity water near the coast may also play a role in the movement of river water back toward the central BoB—this is a question for future research.

Finally, we present observational evidence of the influence of river water on the amplitude of sub-seasonal SST variation. For several weeks in July–September 2015, low-salinity water of riverine origin lies in the northeastern bay, and saltier water lies in the northwestern bay (Figures 8 and 12). We take advantage of this distribution to compare the response of SST to large-scale heat flux within and outside the pool of river water. The net heat flux into the mixed layer has clear 20–25 days variability in both fresh and salty regions (peak-to-peak $-100\ \mathrm{Wm}^{-2}$ to $+100\ \mathrm{Wm}^{-2}$) during active and suppressed monsoon convection. SST, however, responds to heat flux with a distinctly amplified signal on quasi-biweekly timescale in the fresh region, mainly because the mixed layer is less than 10 m deep in the presence of river water.

A narrow-band quasi-biweekly variability has been reported from the equatorial Indian Ocean—analysis of observed ocean currents shows that equatorially trapped mixed Rossby-gravity waves are excited as a resonant response to quasi-biweekly wind stress forcing (Miyama et al., 2006; Sengupta et al., 2004). As mentioned earlier, recent satellite observations show quasi-biweekly variability in BoB SSS (Roman-Stork et al., 2019; Subrahmanyam et al., 2018; Trott et al., 2019). In this study, we focus on the mechanisms that drive quasi-biweekly variability in the north BoB. Moored measurements, satellite data and reanalyses reveal the close connections between the quasi-biweekly mode of the Asian summer monsoon and the variations of surface salinity, sea level, and SST.

The rapid dispersal of low salinity surface water from rivers affects the evolution of SST by modifying mixed layer depth. This finding indicates that a more mechanistic understanding of these oceanic processes in the BoB is crucial in improved forecasting of SST and monsoon variability. We have shown that sub-seasonal SST response to heat flux is amplified twofold in the presence of a thin, fresh surface layer. Most coupled ocean-atmosphere models have serious biases in the simulation of monsoon intraseasonal oscillations due to misrepresentation of regional air-sea interaction (Li et al., 2018; Samanta et al., 2018). The observations indicate the need for ocean models with improved representation of the shallow wind-driven currents and thin mixed layers in the BoB.

Data Availability Statement

INCOIS and NIOT mooring data are available at odis.incois.gov.in/index.php/in-situ-data/all-insitu, and WHOI mooring data at uop.whoi.edu/projects/Bengal/QCData. We acknowledge the following data sources: SMAP SSS www.remss.com/missions/smap/; MW OISST www.remss.com; TropFlux incois.gov.in/tropflux; TRMM 3B42v7 precipitation pmm.nasa.gov/data-access/downloads/trmm; AVISO geostrophic currents www.aviso.altimetry.fr/en/data/; MERRA2 reanalysis winds gmao.gsfc.nasa.gov/reanalysis/MERRA-2, and Global_Analysis_Forecast_PHY_001_030 marine.copernicus.eu/.

Acknowledgments
The authors thank the Ministry of Earth Sciences (MoES) institutes NIOT and INCOIS, and the Upper Ocean Processes (UOP) group at WHOI for design, integration, and deployment of moorings in the BoB. The WHOI mooring was deployed from the ORV *Sagar Nidhi* and recovered from the ORV *Sagar Kanya*—we thank the officers, crew and science teams on the cruises for their support. Sengupta, Ravichandran and Sukhatme acknowledge MoES and the National Monsoon Mission, Indian Institute of Tropical Meteorology (IITM), Pune, for support; Lucas and Farrar acknowledge the US Office of Naval Research for support of ASIRI through grants N00014-13-1-0489, N0001413-100453, N0001417-12880. We thank S. Shivaprasad, Dipanjan Chaudhuri and Jared Buckley for discussion on ocean currents and Ekman flow, and Fabien Durand for discussion on sea level. JSL would like to thank the Divecha Center for Climate Change, IISc., for support. DS acknowledges support from the Department of Science and Technology (DST), New Delhi, under the Indo-Spanish Programme.

References

Agarwal, N., Sharma, R., Basu, S., Parekh, A., Sarkar, A., & Agarwal, V. K. (2007). Bay of Bengal summer monsoon 10–20 day variability in sea surface temperature using model and observations. *Geophysical Research Letters*, *34*(6). https://doi.org/10.1029/2007GL029296

Akhil V. P., Durand F., Lengaigne M., Vialard J., Keerthi M. G., Gopalakrishna V. V., et al. (2014). A modeling study of the processes of surface salinity seasonal cycle in the Bay of Bengal. *Journal of Geophysical Research: Oceans*, *119*, (6), 3926–3947. https://doi.org/10.1002/2013jc009632

Akhil, V. P., Lengaigne, M., Vialard, J., Durand, F., Keerthi, M. G., Chaitanya, A. V. S., et al. (2016). A modeling study of processes controlling the B ay of B engal sea surface salinity interannual variability. *Journal of Geophysical Research: Oceans*, *121*(12), 8471–8495.

Babu, M. T., Sarma, Y. V. B., Murty, V. S. N., & Vethamony, P. (2003). On the circulation in the Bay of Bengal during northern spring inter-monsoon (March–April 1987). *Deep Sea Research Part II: Topical Studies in Oceanography*, *50*(5), 855–865.

Balaguru, K., Chang, P., Saravanan, R., Leung, L. R., Xu, Z., Li, M., & Hsieh, J. S. (2012). Ocean barrier layers' effect on tropical cyclone intensification. *Proceedings of the National Academy of Sciences*, *109*(36), 14343–14347.

Benshila, R., Durand, F., Masson, S., Bourdallé-Badie, R., de Boyer Montégut, C., Papa, F., & Madec, G. (2014). The upper Bay of Bengal salinity structure in a high-resolution model. *Ocean Modelling*, *74*, 36–52.

Buckley, J. M., Mingels, B., & Tandon, A. (2020). The impact of lateral advection on SST and SSS in the northern Bay of Bengal during 2015. *Deep Sea Research Part II: Topical Studies in Oceanography*, *172*, 104653.

Carmack, E., McLaughlin, F., Yamamoto-Kawai, M., Itoh, M., Shimada, K., Krishfield, R., & Proshutinsky, A. (2008). *Freshwater storage in the Northern Ocean and the special role of the Beaufort Gyre in Arctic–subArctic ocean fluxes*. Springer. pp. 145–169.

Chaitanya, A. V. S., Durand, F., Mathew, S., Gopalakrishna, V. V., Papa, F., Lengaigne, M., et al. (2015). Observed year-to-year sea surface salinity variability in the Bay of Bengal during the 2009–2014 period. *Ocean Dynamics*, *65*(2), 173–186.

Chassignet, E. P.,Pascual, A.,Tintoré, J., & Verron, J., (Eds.). (2018). *New frontiers in operational oceanography*. GODAE OceanView. p. 815.

Chatterjee, P., & Goswami, B. N. (2004). Structure, genesis and scale selection of the tropical quasi-biweekly mode. *Quarterly Journal of the Royal Meteorological Society*, *130*(599), 1171–1194.

Chaudhuri, D., Sengupta, D., D'Asaro, E., Venkatesan, R., & Ravichandran, M. (2019). Response of the salinity-stratified Bay of Bengal to cyclone Phailin. *Journal of Physical Oceanography*, *49*(5), 1121–1140.
Chen, T. C., & Chen, J. M. (1993). The 10–20-day mode of the 1979 Indian monsoon: Its relation with the time variation of monsoon rainfall. *Monthly Weather Review*, *121*(9), 2465–2482.
Chen, G., & Sui, C. H. (2010). Characteristics and origin of quasi-biweekly oscillation over the western North Pacific during boreal summer. *Journal of Geophysical Research*, *115*(D14). https://doi.org/10.1029/2009JD013389
Dai, A., & Trenberth, K. E. (2002). Estimates of freshwater discharge from continents: Latitudinal and seasonal variations. *Journal of Hydrometeorology*, *3*(6), 660–687.
DeMott, C. A., Stan, C., Randall, D. A., & Branson, M. D. (2014). Intraseasonal variability in coupled GCMs: The roles of ocean feedbacks and model physics. *Journal of Climate*, *27*(13), 4970–4995.
Diansky, N. A., Zalesny, V. B., Moshonkin, S. N., & Rusakov, A. S. (2006). High resolution modeling of the monsoon circulation in the Indian Ocean. *Oceanology*, *46*(5), 608–628.
Duncan, B., & Han, W. (2009). Indian Ocean intraseasonal sea surface temperature variability during boreal summer: Madden-Julian Oscillation versus submonthly forcing and processes. *Journal of Geophysical Research*, *114*(C5). https://doi.org/10.1029/2008JC004958
Durand, F., Alory, G., Dussin, R., & Reul, N. (2013). SMOS reveals the signature of Indian Ocean Dipole events. *Ocean Dynamics*, *63*(11–12), 1203–1212.
Fekete, B. M., Vörösmarty, C. J., & Grabs, W. (2002). High-resolution fields of global runoff combining observed river discharge and simulated water balances. *Global Biogeochemical Cycles*, *16*(3), 15-1.
Fore, A. G., Yueh, S. H., Tang, W., Stiles, B. W., & Hayashi, A. K. (2016). Combined active/passive retrievals of ocean vector wind and sea surface salinity with SMAP. *IEEE Transactions on Geoscience and Remote Sensing*, *54*(12), 7396–7404.
Fournier, S., Vialard, J., Lengaigne, M., Lee, T., Gierach, M. M., & Chaitanya, A. V. S. (2017). Modulation of the Ganges-Brahmaputra River plume by the Indian Ocean dipole and eddies inferred from satellite observations. *Journal of Geophysical Research: Oceans*, *122*(12), 9591–9604.
Fujinami, H., Yasunari, T., & Morimoto, A. (2014). Dynamics of distinct intraseasonal oscillation in summer monsoon rainfall over the Meghalaya–Bangladesh–western Myanmar region: Covariability between the tropics and mid-latitudes. *Climate Dynamics*, *43*(7–8), 2147–2166.
Fu, X., Wang, B., Li, T., & McCreary, J. P. (2003). Coupling between northward-propagating, intraseasonal oscillations and sea surface temperature in the Indian Ocean. *Journal of the Atmospheric Sciences*, *60*(15), 1733–1753.
Fu, X., Wang, B., Waliser, D. E., & Tao, L. (2007). Impact of atmosphere–ocean coupling on the predictability of monsoon intraseasonal oscillations. *Journal of the Atmospheric Sciences*, *64*(1), 157–174.
Gadgil, S. (2003). The Indian monsoon and its variability. *Annual Review of Earth and Planetary Sciences*, *31*(1), 429–467.
Gangopadhyay, A., Bharat Raj, G. N., Chaudhuri, A. H., Babu, M. T., & Sengupta, D. (2013). On the nature of meandering of the springtime western boundary current in the Bay of Bengal. *Geophysical Research Letters*, *40*(10), 2188–2193.
Gelaro, R., McCarty, W., Suárez, M. J., Todling, R., Molod, A., Takacs, L., et al. (2017). The modern-era retrospective analysis for research and applications, version 2 (MERRA-2). *Journal of Climate*, *30*(14), 5419–5454.
Gentemann, C. L., Wentz, F. J., Mears, C. A., & Smith, D. K. (2004). In situ validation of Tropical Rainfall Measuring Mission microwave sea surface temperatures. *Journal of Geophysical Research*, *109*(C4). https://doi.org/10.1029/2003JC002092
Gordon, A. L., Shroyer, E. L., Mahadevan, A., Sengupta, D., & Freilich, M. (2016). Bay of Bengal: 2013 northeast monsoon upper-ocean circulation. *Oceanography*, *29*(2), 82–91.
Goswami, B. N. (2012). South Asian monsoon. In W. K. M., Lau & D. E., Waliser (Eds.), *Intraseasonal variability in the atmosphere-ocean climate system* (pp. 21 -72). Berlin, Heidelberg: Springer.
Goswami, B. N., Ajayamohan, R. S., Xavier, P. K., & Sengupta, D. (2003). Clustering of synoptic activity by Indian summer monsoon intraseasonal oscillations. *Geophysical Research Letters*, *30*(8). https://doi.org/10.1029/2002GL016734
Grunseich, G., Subrahmanyam, B., & Wang, B. (2013). The Madden-Julian oscillation detected in Aquarius salinity observations. *Geophysical Research Letters*, *40*(20), 5461–5466.
Han, W., Liu, W. T., & Lin, J. (2006). Impact of atmospheric submonthly oscillations on sea surface temperature of the tropical Indian Ocean. *Geophysical Research Letters*, *33*(3). https://doi.org/10.1029/2005GL025082
Huffman, G. J., Bolvin, D. T., Nelkin, E. J., Wolff, D. B., Adler, R. F., Gu, G., et al. (2007). The TRMM multisatellite precipitation analysis (TMPA): Quasi-global, multiyear, combined-sensor precipitation estimates at fine scales. *Journal of Hydrometeorology*, *8*(1), 38–55.
IMD. (2015). *Cyclonic storm Komen over the Bay of Bengal (26 July–02 August, 2015): A report*. Indian Meteorological Department. p. 49.
IMD Monsoon Report. (2015). *A research report on the 2015 southwest monsoon*. Indian Meteorological Department. p. 78.
Joseph, P. V., & Sabin, T. P. (2008). An ocean–atmosphere interaction mechanism for the active break cycle of the Asian summer monsoon. *Climate Dynamics*, *30*(6), 553–566.
Joseph, P. V., & Sijikumar, S. (2004). Intraseasonal variability of the low-level jet stream of the Asian summer monsoon. *Journal of Climate*, *17*(7), 1449–1458.
Kikuchi, K., & Wang, B. (2009). Global perspective of the quasi-biweekly oscillation. *Journal of Climate*, *22*(6), 1340–1359.
Krishnamurti, T. N., & Bhalme, H. N. (1976). Oscillations of a monsoon system. Part I. Observational aspects. *Journal of the Atmospheric Sciences*, *33*(10), 1937–1954.
Krishnamurti, T. N., Jayakumar, P. K., Sheng, J., Surgi, N., & Kumar, A. (1985). Divergent circulations on the 30 to 50 day timescale. *Journal of the Atmospheric Sciences*, *42*(4), 364–375.
Kumar, P. H., Kumar, N. M., Shyni, T. N., & Rao, A. R. (2013). Observed variability of thermohaline fields, currents and eddies in the western Bay of Bengal during BOBMEX-99. *Marine Geodesy*, *36*(2), 219–233.
Kumar, B. P., Vialard, J., Lengaigne, M., Murty, V. S. N., & McPhaden, M. J. (2012). TropFlux: air-sea fluxes for the global tropical oceans—description and evaluation. *Climate Dynamics*, *38*(7–8), 1521–1543.
Li, Y., Han, W., Ravichandran, M., Wang, W., Shinoda, T., & Lee, T. (2017a). Bay of Bengal salinity stratification and Indian summer monsoon intraseasonal oscillation: 1. Intraseasonal variability and causes. *Journal of Geophysical Research: Oceans*, *122*(5), 4291–4311.
Li, Y., Han, W., Wang, W., Ravichandran, M., Lee, T., & Shinoda, T. (2017b). Bay of Bengal salinity stratification and Indian summer monsoon intraseasonal oscillation: 2. Impact on SST and convection. *Journal of Geophysical Research: Oceans*, *122*(5), 4312–4328.
Li, Y., Han, W., Wang, W., Zhang, L., & Ravichandran, M. (2018). The Indian summer monsoon intraseasonal oscillations in CFSv2 forecasts: Biases and importance of improving air-sea interaction processes. *Journal of Climate*.*31*, 5351–5370.

Lucas, A. J., Nash, J. D., Pinkel, R., MacKinnon, J. A., Tandon, A., Mahadevan, A., et al. (2016). Adrift upon a salinity-stratified sea: A view of upper-ocean processes in the Bay of Bengal during the southwest monsoon. *Oceanography, 29*(2). https://www.jstor.org/stable/24862677

Miyama, T., McCreary, J. P., Jr, Sengupta, D., & Senan, R. (2006). Dynamics of biweekly oscillations in the equatorial Indian Ocean. *Journal of Physical Oceanography*, *36*(5), 827–846.

Mohapatra, M., Geetha, B., Balachandran, S., & Rathore, L. S. (2015). On the tropical cyclone activity and associated environmental features over north Indian Ocean in the context of climate change. *Journal of Climate Change*, *1*(1, 2), 1–26.

Murty, V. S. N., Sarma, Y. V. B., Rao, D. P., & Murty, C. S. (1992). Water characteristics, mixing and circulation in the Bay of Bengal during southwest monsoon. *Journal of Marine Research*, *50*(2), 207–228.

Neetu, S., Lengaigne, M., Vincent, E. M., Vialard, J., Madec, G., Samson, G., et al. (2012). Influence of upper-ocean stratification on tropical cyclone-induced surface cooling in the Bay of Bengal. *Journal of Geophysical Research*, *117*(C12). https://doi.org/10.1029/2012JC008433

Pant, V., Girishkumar, M. S., Bhaskar, T. U., Ravichandran, M., Papa, F., & Thangaprakash, V. P. (2015). Observed interannual variability of near-surface salinity in the Bay of Bengal. *Journal of Geophysical Research: Oceans*, *120*(5), 3315–3329. https://doi.org/10.1002/2014JC010340

Papa, F., Bala, S. K., Pandey, R. K., Durand, F., Gopalakrishna, V. V., Rahman, A., & Rossow, W. B. (2012). Ganga-Brahmaputra river discharge from Jason-2 radar altimetry: An update to the long-term satellite-derived estimates of continental freshwater forcing flux into the Bay of Bengal. *Journal of Geophysical Research*, *117*(C11). https://doi.org/10.1029/2012JC008158

Papa, F., Durand, F., Rossow, W. B., Rahman, A., & Bala, S. K. (2010). Satellite altimeter-derived monthly discharge of the Ganga-Brahmaputra River and its seasonal to interannual variations from 1993 to 2008. *Journal of Geophysical Research*, *115*(C12). https://doi.org/10.1029/2009JC006075

Parampil, S. R., Bharathraj, G. N., Harrison, M., & Sengupta, D. (2016). Observed subseasonal variability of heat flux and the SST response of the tropical Indian Ocean. *Journal of Geophysical Research: Oceans*, *121*(10), 7290–7307. https://doi.org/10.1002/2016JC011948

Parampil, S. R., Gera, A., Ravichandran, M., & Sengupta, D. (2010). Intraseasonal response of mixed layer temperature and salinity in the Bay of Bengal to heat and freshwater flux. *Journal of Geophysical Research*, *115*(C5). https://doi.org/10.1029/2009JC005790

Parekh, A., Sarkar, A., Shah, S., & Narayanan, M. S. (2004). Low period variability in tropical rainfall measuring mission microwave imager measured sea surface temperature over the Bay of Bengal during summer monsoon. *Current Science*, *87*(6), 791–796.

Paulson, C. A., & Simpson, J. J. (1977). Irradiance measurements in the upper ocean. *Journal of Physical Oceanography*, *7*(6), 952–956.

Paul, N., & Sukhatme, J. (2020). Seasonality of surface stirring by geostrophic flows in the Bay of Bengal. *Deep Sea Research Part II: Topical Studies in Oceanography*, *172*, 104684. https://doi.org/10.1016/j.dsr2.2019.104684

Prend, C. J., Seo, H., Weller, R. A., Farrar, J. T. (2019). Impact of freshwater plumes on intraseasonal upper ocean variability in the Bay of Bengal. *Deep Sea Research Part II: Topical Studies in Oceanography*, *161*, 63–71. https://doi.org/10.1016/j.dsr2.2018.09.007

Qiu, Y., Han, W., Lin, X., West, B. J., Li, Y., Xing, W., et al. (2019). Upper-ocean response to the super tropical cyclone Phailin (2013) over the freshwater region of the Bay of Bengal. *Journal of Physical Oceanography*, *49*(5), 1201–1228.

Rao, S. A., Saha, S. K., Pokhrel, S., Sundar, D., Dhakate, A. R., Mahapatra, S., et al. (2011). Modulation of SST, SSS over northern Bay of Bengal on ISO timescale. *Journal of Geophysical Research*, *116*(C9). https://doi.org/10.1029/2010JC006804

Rao, R. R., & Sivakumar, R. (2003). Seasonal variability of sea surface salinity and salt budget of the mixed layer of the north Indian Ocean. *Journal of Geophysical Research*, *108*(C1), 9-1. https://doi.org/10.1029/2001JC000907

Roman-Stork, H. L., Subrahmanyam, B., Murty, V. S. N. (2019). Quasi-biweekly oscillations in the Bay of Bengal in observations and model simulations. *Deep Sea Research Part II: Topical Studies in Oceanography*, *168*, 104609. https://doi.org/10.1016/j.dsr2.2019.06.017

Saji, N. H., Goswami, B. N., Vinayachandran, P. N., & Yamagata, T. (1999). A dipole mode in the tropical Indian Ocean. *Nature*, *401*(6751), 360.

Samanta, D., Hameed, S. N., Jin, D., Thilakan, V., Ganai, M., Rao, S. A., & Deshpande, M. (2018). Impact of a narrow coastal Bay of Bengal sea surface temperature front on an Indian summer monsoon simulation. *Scientific Reports*, *8*(1), 17694.

Schott, F. A., Xie, S. P., & McCreary, J. P., Jr (2009). Indian Ocean circulation and climate variability. *Reviews of Geophysics*, *47*(1). https://doi.org/10.1029/2007RG000245

Sengupta, D., Bharath Raj, G. N., Ravichandran, M., Sree Lekha, J., & Papa, F. (2016). Near-surface salinity and stratification in the north Bay of Bengal from moored observations. *Geophysical Research Letters*, *43*(9), 4448–4456. https://doi.org/10.1002/2016GL068339

Sengupta, D., Bharath Raj, G. N., & Shenoi, S. S. C. (2006). Surface freshwater from Bay of Bengal runoff and Indonesian throughflow in the tropical Indian Ocean. *Geophysical Research Letters*, *33*(22). https://doi.org/10.1029/2006GL027573

Sengupta, D., Goddalehundi, B. R., & Anitha, D. S. (2008). Cyclone-induced mixing does not cool SST in the post-monsoon North Bay of Bengal. *Atmospheric Science Letters*, *9*(1), 1–6. https://doi.org/10.1002/asl.162

Sengupta, D., & Ravichandran, M. (2001). Oscillations of Bay of Bengal sea surface temperature during the 1998 summer monsoon. *Geophysical Research Letters*, *28*(10), 2033–2036. https://doi.org/10.1029/2000GL012548

Sengupta, D., Ray, P. K., & Bhat, G. S. (2002). Spring warming of the eastern Arabian Sea and Bay of Bengal from buoy data. *Geophysical Research Letters*, *29*(15), 24-1. https://doi.org/10.1029/2002GL015340

Sengupta, D., Senan, R., Murty, V. S. N., & Fernando, V. (2004). A biweekly mode in the equatorial Indian Ocean. *Journal of Geophysical Research*, *109*(C10). https://doi.org/10.1029/2004JC002329

Shankar, D., Shetye, S. R., & Joseph, P. V. (2007). Link between convection and meridional gradient of sea surface temperature in the Bay of Bengal. *Journal of Earth System Science*, *116*(5), 385–406.

Shenoi, S. S. C., Shankar, D., & Shetye, S. R. (2002). Differences in heat budgets of the near-surface Arabian Sea and Bay of Bengal: Implications for the summer monsoon. *Journal of Geophysical Research*, *107*(C6), 5-1. https://doi.org/10.1029/2000JC000679

Shetye, S. R., Gouveia, A. D., Shankar, D., Shenoi, S. S. C., Vinayachandran, P. N., Sundar, D., et al. (1996). Hydrography and circulation in the western Bay of Bengal during the northeast monsoon. *Journal of Geophysical Research*, *101*(C6), 14011–14025.

Shetye, S. R., Gouveia, A. D., Shenoi, S. S. C., Sundar, D., Michael, G. S., & Nampoothiri, G. (1993). The western boundary current of the seasonal subtropical gyre in the Bay of Bengal. *Journal of Geophysical Research*, *98*(C1), 945–954.

Shroyer, E. L., Gordon, A. L., Jaeger, G. S., Freilich, M., Waterhouse, A. F., Farrar, J. T., et al. (2020). Upper layer thermohaline structure of the Bay of Bengal during the 2013 northeast monsoon. *Deep Sea Research Part II: Topical Studies in Oceanography*, *172*, 104630.

Sree Lekha, J., Buckley, J. M., Tandon, A., & Sengupta, D. (2018). Subseasonal dispersal of freshwater in the northern Bay of Bengal in the 2013 summer monsoon season. *Journal of Geophysical Research: Oceans*, *123*(9), 6330–6348. https://doi.org/10.1029/2018JC014181

Steele, M., Thomas, D., Rothrock, D., & Martin, S. (1996). A simple model study of the Arctic Ocean freshwater balance, 1979–1985. *Journal of Geophysical Research: Oceans*, *101*(C9), 20833–20848.

Subrahmanyam, B., Trott, C. B., & Murty, V. S. N. (2018). Detection of intraseasonal oscillations in SMAP salinity in the Bay of Bengal. *Geophysical Research Letters*, *45*(14), 7057–7065. https://doi.org/10.1029/2018GL078662

Thadathil, P., Suresh, I., Gautham, S., Prasanna Kumar, S., Lengaigne, M., Rao, R. R., et al. (2016). Surface layer temperature inversion in the Bay of Bengal: Main characteristics and related mechanisms. *Journal of Geophysical Research: Oceans*, *121*(8), 5682–5696.

Trott, C. B., Subrahmanyam, B., Roman-Stork, H. L., Murty, V. S. N., & Gnanaseelan, C. (2019). Variability of intraseasonal oscillations and synoptic signals in sea surface salinity in the Bay of Bengal. *Journal of Climate*, *32*(20), 6703–6728.

Udaya Bhaskar, T. V., Jayaram, C., & Rama Rao, E. P. (2013). Comparison between Argo-derived sea surface temperature and microwave sea surface temperature in tropical Indian Ocean. *Remote Sensing Letters*, *4*(2), 141–150.

Vecchi, G. A., & Harrison, D. E. (2002). Monsoon breaks and subseasonal sea surface temperature variability in the Bay of Bengal. *Journal of Climate*, *15*(12), 1485–1493.

Venkatesan, R., Shamji, V. R., Latha, G., Mathew, S., Rao, R. R., Muthiah, A., & Atmanand, M. A. (2013). In situ ocean subsurface time-series measurements from OMNI buoy network in the Bay of Bengal. *Current Science*, 1166–1177.

Vialard, J., Jayakumar, A., Gnanaseelan, C., Lengaigne, M., Sengupta, D., & Goswami, B. N. (2012). Processes of 30–90 days sea surface temperature variability in the northern Indian Ocean during boreal summer. *Climate Dynamics*, *38*(9–10), 1901–1916.

Vinayachandran, P. N., Murty, V. S. N., & Ramesh Babu, V. (2002). Observations of barrier layer formation in the Bay of Bengal during summer monsoon. *Journal of Geophysical Research*, *107*(C12), SRF-19. https://doi.org/10.1029/2001JC000831

Vincent, E. M., Emanuel, K. A., Lengaigne, M., Vialard, J., & Madec, G. (2014). Influence of upper ocean stratification interannual variability on tropical cyclones. *Journal of Advances in Modeling Earth Systems*, *6*(3), 680–699.

Wang, X., & Chen, G. (2017). Quasi-biweekly oscillation over the south China sea in late summer: Propagation dynamics and energetics. *Journal of Climate*, *30*(11), 4103–4112.

Wang, B., Huang, F., Wu, Z., Yang, J., Fu, X., & Kikuchi, K. (2009). Multi-scale climate variability of the south China sea monsoon: A review. *Dynamics of Atmospheres and Oceans*, *47*(1–3), 15–37.

Wang, X., & Zhang, G. J. (2019). Evaluation of the quasi-biweekly oscillation over the south China sea in early and late summer in CAM5. *Journal of Climate*, *32*(1), 69–84.

Webster, P. J., Moore, A. M., Loschnigg, J. P., & Leben, R. R. (1999). Coupled ocean–atmosphere dynamics in the Indian Ocean during 1997–98. *Nature*, *401*(6751), 356.

Weller, R. A., Farrar, J. T., Buckley, J., Mathew, S., Venkatesan, R., Lekha, J. S., et al. (2016). Air-sea interaction in the Bay of Bengal. *Oceanography*, *29*(2), 28–37.

Weller, R. A., Farrar, J. T., Seo, H., Prend, C., Sengupta, D., Lekha, J. S., et al. (2019). Moored observations of the surface meteorology and air-sea fluxes in the northern Bay of Bengal in 2015. *Journal of Climate*, *32*, 549–573.

Wilson, E. A., & Riser, S. C. (2016). An assessment of the seasonal salinity budget for the upper Bay of Bengal. *Journal of Physical Oceanography*, *46*(5), 1361–1376.